

# Characterization of Solar X-ray Response Data from the REXIS Instrument

by

Andrew T. Cummings

Submitted to the Department of Earth, Atmospheric, and Planetary  
Sciences

in partial fulfillment of the requirements for the degree of

Bachelor of Science in Earth, Atmospheric, and Planetary Sciences

at the

MASSACHUSETTS INSTITUTE OF TECHNOLOGY

June 2020

© Massachusetts Institute of Technology 2020. All rights reserved.

Author .....

Department of Earth, Atmospheric, and Planetary Sciences

May 18, 2020

Certified by .....

Richard P. Binzel

Professor of Planetary Sciences

Thesis Supervisor

Certified by .....

Rebecca A. Masterson

Principal Research Scientist

Thesis Supervisor

Accepted by .....

Richard P. Binzel

Undergraduate Officer, Department of Earth, Atmospheric, and

Planetary Sciences



# Characterization of Solar X-ray Response Data from the REXIS Instrument

by

Andrew T. Cummings

Submitted to the Department of Earth, Atmospheric, and Planetary Sciences  
on May 18, 2020, in partial fulfillment of the  
requirements for the degree of  
Bachelor of Science in Earth, Atmospheric, and Planetary Sciences

## **Abstract**

The REgolith X-ray Imaging Spectrometer (REXIS) is a student-built instrument that was flown on NASA's Origins, Spectral Interpretation, Resource Identification, Safety, Regolith Explorer (OSIRIS-REx) mission. During the primary science observation phase, the REXIS Solar X-ray Monitor (SXM) experienced a lower than anticipated solar x-ray count rate. Solar x-ray count decreased most prominently in the low energy region of instrument detection, and made calibrating the REXIS main spectrometer difficult. This thesis documents a root cause investigation into the cause of the low x-ray count anomaly in the SXM. Vulnerable electronic components are identified, and recommendations for hardware improvements are made to better facilitate future low-cost, high-risk instrumentation.

Thesis Supervisor: Richard P. Binzel  
Title: Professor of Planetary Sciences

Thesis Supervisor: Rebecca A. Masterson  
Title: Principal Research Scientist



# Acknowledgments

I conducted my work as a research assistant with the REXIS program in the Space Systems Laboratory as a student in the MIT Department of Earth, Atmospheric, and Planetary Sciences and the MIT Department of Aeronautics and Astronautics. I owe this thesis to the dedication of countless friends, loved ones, faculty, and staff. Though there are too many to list, I wish to acknowledge a few:

First and foremost, I would like to express my gratitude to Dr. Rebecca Masterson for her guidance and encouragement in the past year. Thank you for always challenging me to grow and improve as an engineer, and for always believing in me.

I would like to thank my other advisor, Professor Richard Binzel, who first invited me to join the REXIS project, and whose passion for science motivated me to dream big and start down this road. Thank you for recognizing something in me, and for agreeing to advise just one last time. Additionally like to recognize the Harvard-Smithsonian Center for Astrophysics team of Dr. Branden Allen, Dr. Daniel Hoak, Dr. Jaesub Hong, and Professor Jonathan Grindlay for mentoring me. Many thanks to the REXIS cohort of Maddy Lambert, Carolyn Thayer, and David Guevel; I would do it all again for the laughs and camaraderie. Special thanks to Megan Jordan for tolerating endless paperwork and logistics, and at times, wrangling me in.

I would also like to thank my family for sending their love and support from so very far away. And to my friends: Lucy, Dan, Brandon, Ruth, Brendan, and Lara; Thank you for being the people who lifted me up when I was down, and for being with me all the way.

Lastly, I wish to thank the Halperin family, for welcoming me into their home during an unprecedented global crisis.



# Contents

<b>1</b>	<b>Introduction</b>	<b>13</b>
1.1	REXIS Mission . . . . .	14
1.2	REXIS Operational Timeline . . . . .	16
1.3	Anomaly Resolution during the OSIRIS-REx mission . . . . .	17
1.4	Motivation . . . . .	18
1.5	Thesis Roadmap . . . . .	19
<b>2</b>	<b>Background</b>	<b>21</b>
2.1	Basic Circuitry . . . . .	22
2.1.1	Common Components . . . . .	22
2.1.2	Operational Amplifiers . . . . .	25
2.1.3	Signal Amplification . . . . .	27
2.1.4	Analog-to-Digital Signal Conversion . . . . .	29
2.1.5	Thermal Impact on Circuitry . . . . .	30
2.2	SXM Overview . . . . .	31
2.3	SXM Data Pipeline . . . . .	32
2.3.1	Instrument Response Modeling . . . . .	32
2.3.2	Chianti Atomic Database . . . . .	32
<b>3</b>	<b>SXM Design and Operation</b>	<b>33</b>
3.1	SXM Design Background . . . . .	34
3.1.1	Mission Requirements . . . . .	35
3.1.2	Overview of SXM Signal Amplification Chain . . . . .	37

3.2	Instrument Testing . . . . .	42
3.2.1	Ground Testing . . . . .	42
3.3	Flight Operations . . . . .	45
3.3.1	Early Flight Operations . . . . .	45
3.3.2	Flight Operations during Orbital B . . . . .	46
3.3.3	Flight Operations during Orbital R . . . . .	47
<b>4</b>	<b>SXM Root Cause Analysis</b>	<b>51</b>
4.1	SXM Low Count Rate Anomaly . . . . .	52
4.1.1	Orbital B . . . . .	52
4.1.2	Orbital R . . . . .	54
4.2	Constraining the Problem . . . . .	54
4.2.1	ISA #10939 . . . . .	55
4.2.2	Modeling SXM Instrument Response . . . . .	60
4.3	LTSpice Simulations of Amplification Chain . . . . .	61
4.3.1	Thermal Variability in Components . . . . .	62
4.4	Root Cause Next Steps . . . . .	65
4.4.1	Identification of Vulnerable Components . . . . .	65
4.4.2	CAST Analysis . . . . .	65
<b>A</b>	<b>SXM Circuit Schematics</b>	<b>69</b>
<b>B</b>	<b>Simulation Code</b>	<b>103</b>
B.1	SXM Simulated Instrument Response Code . . . . .	103
B.2	SXM Histogram Rebinning . . . . .	107
B.3	LTSpice Simulation Readout . . . . .	114



# List of Figures

1-1	Schematic of the REXIS Instrument and SXM (shown to scale). . . . .	15
2-1	The symbol used to represent a resistor in circuit diagrams. . . . .	22
2-2	The symbol used to represent a capacitor in circuit diagrams. . . . .	23
2-3	The symbol used to represent a diode in circuit diagrams. The positive terminal is to the left, and the negative terminal is on the right. . . . .	24
2-4	A generic op-amp. (1) Inverting input, (2) Non-inverting input, (3) Positive power supply, (4) Negative power supply, (5) Output. . . . .	25
2-5	A generic op-amp with open-loop gain. . . . .	26
2-6	A generic op-amp with closed-loop gain. . . . .	27
2-7	An example differentiator circuit. . . . .	28
2-8	An example integrator circuit. . . . .	28
2-9	An integrator circuit with an additional resistor added to the feedback loop provides a discharge path for the capacitor. . . . .	29
2-10	An example Schmitt Trigger. . . . .	30
3-1	The REXIS Requirements documentation flow from Jones, 2015 [6].	35
3-2	SXM detector and preamp housing. The SXM detector is located below the collimator. . . . .	38
3-3	Schematic of SXM Amplification Chain. Outputs <i>outb</i> and <i>outu</i> are seen on the far right. . . . .	39
3-4	SXM Trigger Circuit Schematic. . . . .	40
3-5	SXM signals at various points throughout the amplification chain. . .	41

3-6	SXM Histogram of Ground Calibration Source. A strong iron line can be seen at around 200 ADU. . . . .	43
3-7	Results of SXM Oven Test, November 2015. . . . .	44
3-8	Temperature Fluctuations during the MEB Thermal Characterization Test. . . . .	44
3-9	Ground Testing results of MEB susceptibility to temperature fluctuations. . . . .	45
3-10	SXM Event Rate Histograms during L+30 . . . . .	47
3-11	SXM Event Rate Histogram from Orbital B, 25 July 2019. . . . .	48
3-12	SXM Event Rate Histogram from Orbital R, 13 November 2019. . . . .	49
4-1	Example Fishbone diagram used to outline a Root Cause Analysis. Each bone is used to categorize the type of cause. . . . .	51
4-2	SXM count rate histogram from launch to Orbital R. . . . .	53
4-3	SXM Saturated Histogram (Right) and Corrected Histogram (Left) . . . . .	54
4-4	SXM count rate histogram on 18 November, 2019. The gap in the histogram is when the instrument was not recording data, and is unrelated to the low count rate anomaly in Orbital R. . . . .	55
4-5	Fishbone diagram constructed for OSIRIS-REx ISA #10939 . . . . .	56
4-6	Flare Coincidence between the SXM and GOES15. . . . .	57
4-7	SXM longterm HV for its operational lifetime. . . . .	58
4-8	SXM Temperature Phase Space. . . . .	59
4-9	SXM Histogram Rebinning. The boxed area surrounds the SXM's main signal peaks. The peaks at the outer edges of the figure are instrument artifacts. . . . .	61
4-10	The SXM Signal Amplification Chain. . . . .	64

# List of Tables

3.1	Quantum Efficiency Requirements for the SXM Detector. . . . .	36
3.2	SXM Level 3 Requirements. . . . .	36
3.3	SXM Level 4 Requirements. . . . .	37



# Chapter 1

## Introduction

This thesis is intended to provide an overview of operations involving the REXIS Solar X-ray Monitor (SXM), and an investigation into the cause of unanticipated low solar signal seen during data collection. The SXM is a subunit of the REgolith X-ray Imaging Spectrometer (REXIS), which is mounted aboard NASA's OSIRIS-REx mission.

REXIS an instrument intended to use to produce elemental abundance maps of the surface of the asteroid 101955 Bennu, a C-type near-Earth asteroid using spectrometry. Bennu is of particular interest because it has a 1-in-2700 chance of impacting Earth between 2175 and 2199 [9].

The SXM is a low-cost, high-risk payload. Isolating the root cause of the malfunction and identifying critical components that resulted in failure will provide future projects with additional knowledge for instrument design. The SXM works in conjunction with the REXIS spectrometer to characterize high-energy solar x-ray flux. The SXM is used to detect variable input from the Sun, which is used by the REXIS spectrometer to calibrate x-ray input to Bennu. This thesis will provide an explanation of how solar x-rays are captured by the SXM and how signal data are interpreted. Solar spectra analysis and solar temperature fitting techniques are discussed, as well as the limitations of SXM modeling. SXM hardware is explained, with a focus on the analog signal amplification chain.

An operational timeline of the SXM will be presented. The focus of the latter por-

tion of the thesis will be on a root cause analysis of the low x-ray count-rate anomaly that occurred late in the SXM's operational lifetime. This thesis will conclude with a roadmap for future work, including a more complete root cause investigation into thermal sensitivity, and a CAST analysis to highlight organizational and programmatic controls that may have contributed to the drop off in x-ray counts.

## 1.1 REXIS Mission

REXIS is a student experiment developed initially as part of the 2011 undergraduate capstone class in the Department of Aeronautics and Astronautics at MIT. Construction and management of the instrument was conducted in the MIT Space Systems Laboratory (SSL) as part of a larger collaboration with Harvard College Observatory (HCO), the MIT Department of Earth, Atmospheric, and Planetary Science, the MIT Kavli Institute (MKI), MIT Lincoln Laboratories, and Aurora Flight Sciences. Day-to-day operations and engineering are conducted primarily by students with guidance from senior faculty and staff including Professor Richard Binzel, the REXIS Instrument Scientist, Professor Jonathan Grindlay, the REXIS Deputy Instrument scientist from HCO, and Dr. Rebecca Masterson, the REXIS Project Manager, from the MIT Department of Aeronautics and Astronautics. To date, over 80 students have worked on REXIS at all levels and stages of the project.

The REXIS main spectrometer relies on coded aperture mask spectroscopy to capture incident x-rays from Bennu's surface in the soft x-ray band (0.5-7.5 keV). A total x-ray spectrum is derived from the soft x-ray data and REXIS was designed to detect, if measurable, signals from Si, S, Mg, and O. REXIS has two operating modes: Imaging and Spectral. In imaging mode, REXIS maps specific abundances to locations on Bennu's surface with necessary spatial resolution at an observation distance of 700m. In spectral mode, REXIS records x-ray energies and produces the global average of the x-ray spectrum passing through the coded aperture mask. REXIS performs its science objective in concert with the other OSIRIS-REx instruments.

The flight schematic of REXIS is shown in Figure 1-1. The primary components

of REXIS are housed in the main instrument. These consist of a 2x2 array of CCD's housed within a coded aperture mask. Housed separately is the Solar X-Ray Monitor (SXM), which will be the focus of this study.

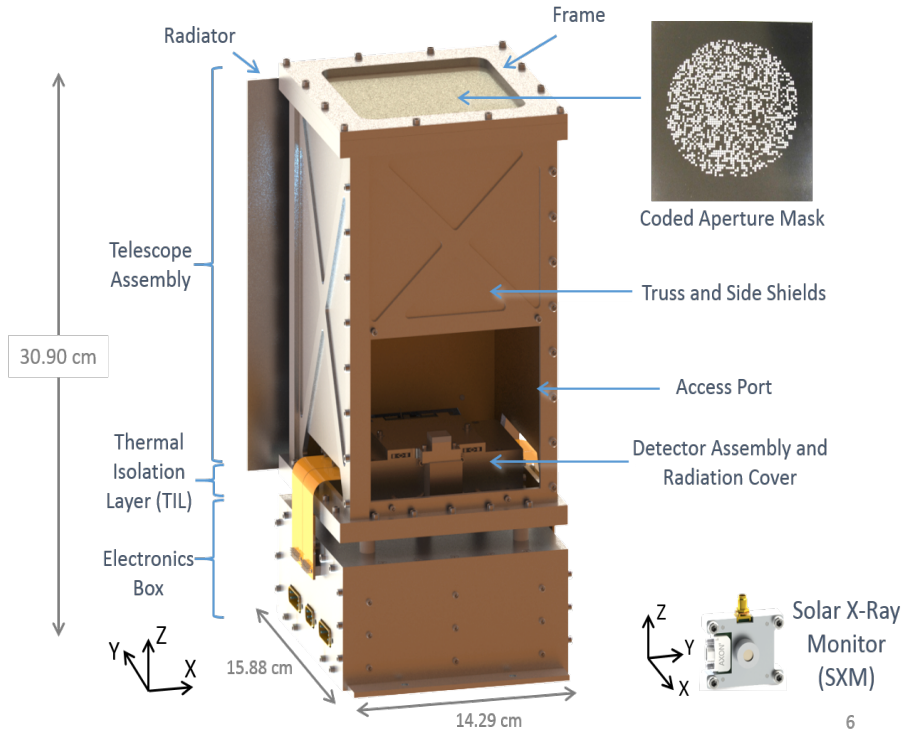


Figure 1-1: Schematic of the REXIS Instrument and SXM (shown to scale).

The SXM is an x-ray detector located on the outside of the spacecraft bus, so that it would be sun facing during observations of Bennu. The SXM is connected to REXIS by a coax cable, and SXM data processing occurs in the main REXIS instrument.

REXIS is the second student experiment to accompany a New Frontiers mission as part of NASA's education and public outreach initiative. The first student instrument, the Venetia Burney Student Dust Counter (VBSDC, formerly SDC) built by University of Colorado Boulder, flew on the New Horizons spacecraft and recorded interplanetary dust from between 2.6 and 15.5 AU [13]. REXIS is a significant leap in complexity from the VBSDC, and at its inception was required to "directly engage students at the undergraduate and graduate levels in the conception, design, implementation, and operation of space flight instrumentation. (2011 internal program

level doc.)"

## 1.2 REXIS Operational Timeline

This section will discuss the operational lifetime of REXIS and the SXM, from its launch on 8 September 2016 until the instrument's planned shutdown following the OSIRIS-REx Orbital R mission phase in November 2019. A more detailed explanation of SXM operations can be found in Chapter 3. Henceforth, some operational times will be referred to as "L+", which stands for months after launch, unless otherwise specified. For example, events in the L+30 phase of the mission occurred 30 months after launch. The REXIS timeline is inherently linked to the OSIRIS-REx timeline.

REXIS was powered on during L+14 Days for a payload inspection and functions check. The SXM took 3935 seconds of x-ray data, and the instrument function was nominal. The SXM was turned on for an additional function check at L+6, where the instrument threshold was set. A third functions check was conducted during L+18. The SXM remained nominal, and there were no anomalies in x-ray detection.

The next big milestone was the L+22 Checkout in July 2018, where REXIS and the SXM were again checked for behavioral anomalies. Data collected by the SXM demonstrated full functionality. During L+22, REXIS was internally calibrated to identify background noise and hot pixels. As a diode detector, the SXM cannot have hot pixels in the same way as a charge-coupled device (CCD) detector.

REXIS performed its cover opening operation in September 2018. The radiation cover was released using a frangibolt, after which REXIS detectors were first exposed to the space environment. REXIS underwent a series of cosmic x-ray calibrations (CXB), and the REXIS spectrometer was shown to be sensitive to stray light.

The L+30 Calibration was the first time Bennu was observable in the REXIS field of view. During this calibration, a hot pixel mask was tested on REXIS. SXM count rates were lower than previous observations, but returned to previously seen levels in later flight.

During flight, REXIS underwent a series of calibrations using the Crab Nebula and



Scorpius X-1 (Sco-X-1), two known cosmic x-ray sources. Using a known, stable x-ray emitter provided a source that allowed the gain and offset of the REXIS detector nodes to be set. Crab Calibration took place in November 2018 and March 2019, while Sco X-1 occurred later, during Mask Calibration.

Orbital B, the first REXIS observation phase, occurred from 1 July to 6 August, 2019. This was initially the only observation window for REXIS. The OSIRIS-REx spacecraft was placed in a stable orbit one kilometer above the surface of Bennu. The SXM count rate saturation anomaly was found during Orbital B, where the instrument reported abnormally high counts on the detector. On 5 July, SXM data was saturated with an additional value of 34880. It was believed that a "bit flip" occurred, where radiation moved the reset value on the SXM. This was corrected with a reset command from the ground.

Additionally, throughout Orbital B the SXM began showing a two order of magnitude decrease in x-ray signal disproportional to the spacecraft's solar distance. The results from results from the SXM's Internal Calibration are depicted in Figure 4-2. More on this anomaly can be found in Chapter 4. In all, two anomalies were detected in the SXM, and three were detected in REXIS. For more information on REXIS anomalies, consult Maddy Lambert's thesis [7].

Orbital R was the final observation window for REXIS, which occurred during November 2019. The REXIS team petitioned for, and was awarded, this additional observation to supplement limited data taken during Orbital B.

### **1.3 Anomaly Resolution during the OSIRIS-REx mission**

Anomaly detection for instruments on OSIRIS-REx was primarily the job of the engineers and scientists behind the individual instrument. Generally, a few weeks were allotted after reporting the anomaly to conduct an investigation, and isolate the root cause.

After an assessment had been made, the instrument team would present a recommendation for how to proceed with using the instrument to the OSIRIS-REx PI. This recommendation included an identification of the incident, current results of the investigation, and conclusions about future instrument performance and how it might affect the spacecraft. The investigation could be closed without reaching a defined root cause, so long as the incident was isolated and did not impact other instruments on the spacecraft.

## 1.4 Motivation

Low-cost, high-risk spaceflight missions granting better accessibility to space than ever before. The REXIS project was developed with the philosophy of being a student instrument. From its inception as the final deliverable for 16.83, the MIT Aerospace Engineering senior design capstone class, where undergraduate students worked side-by-side with experienced research scientists and engineers. Students directly applied s learned in their undergraduate curricula, and produced an instrument of complexity, scale, and mission worthy of being included on a New Frontiers spacecraft. Like all projects, there were challenges faced along the way. A rotating ensemble of students created a challenging environment for informational and experiential entropy.

The REXIS instrument is categorized as a NASA Risk Class D mission, which is characterized by lower cost and the use of legacy hardware [11]. Indeed, a portion of the electronics design process for REXIS consisted of utilizing existing schematics from NICER, an x-ray instrument developed by the MIT Kavli Institute (MKI). These schematics were simplified for the design of the SXM as a matter of reducing cost. Identifying the source of the SXM spaceflight anomaly not only provides guidance on potential hardware vulnerabilities which exist in current spaceflight missions; it also yields a roadmap for future missions.

## 1.5 Thesis Roadmap

This thesis is organized into six chapters, which document the SXM background, instrument anomaly, and subsequent investigation. The current chapter has introduced the larger REXIS mission, operations over its lifetime, and how anomalies were identified, catalogued, and solved. Chapter 2 presents a background on the SXM, including an explanation of the SXM data pipeline and associated solar x-ray modeling. A broad overview of the electronic components that comprise the SXM will be provided, as well as how they operate in the space environment. In Chapter 3, the structure and design process of the SXM will be explained in greater detail. This is followed by a summary of instrument testing that occurred, both on the ground and after launch. Then, SXM flight operations leading up to and after the anomaly are discussed. Chapter 4 explores the SXM root cause analysis. The identification of the low count-rate anomaly is explained in depth. The investigation into the SXM pre-amplification chain electronics is next. The chapter ends with a plan for future research into the identification of the vulnerability that caused the anomaly and how such a finding may be interpreted.



# Chapter 2

## Background

This chapter will describe the circuitry used in the SXM. The SXM relies on an intricate array of amplifiers and filters, which are capable of x-ray detection when combined. The chapter will begin with an introduction of standard electrical components and how they operate. An example circuit of each component is provided and includes a visual representation of ideal operation. This will create a foundation of understanding that will translate to more complex electrical engineering systems seen in the SXM. The first advanced concept explained is signal amplification. Signal amplification is the primary means through which a signal is passed from the SXM detector and recorded by the instrument. Typical amplification techniques will be compared against amplification used in the SXM. To understand signal processing in the SXM, an explanation of analog-to-digital conversion is provided. A more thorough model of SXM signal processing is covered later in the chapter. The thermal sensitivity of electrical systems is explained, and typical response sensitivities are modeled. An overview of the SXM will explain the functions of the instrument in broad terms. The SXM Data Pipeline will be explained from end-to-end. A theoretical solar x-ray response will be followed from detection, through the pipeline, and finally to transmission to the ground. Finally, the chapter concludes with theoretical instrument response using the Chianti Atomic Database and an explanation of how it was implemented in the Data Pipeline. SXM instrument simulation code can be found in Appendix B.

## 2.1 Basic Circuitry

This section introduces the common electrical components used in the SXM, how they operate individually, and how they are used together to create more complex circuitry.

### 2.1.1 Common Components

#### Resistor

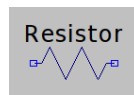


Figure 2-1: The symbol used to represent a resistor in circuit diagrams.

A resistor is an electrical element with a positive and negative terminal that utilizes the property of electrical resistance. Its primary functions include voltage division, current flow reduction, and signal reduction. Ideal resistors function based on Ohm's law,

$$V = IR \quad (2.1)$$

where the voltage differential across the resistor is proportional to the product of current and resistivity. Resistors are commonly used in two constructions: parallel and series. Resistors in parallel are be treated as the multiplicative inverse of the sum of the reciprocals of individual resistors,

$$\frac{1}{R_{eq}} = \frac{1}{R_1} + \frac{1}{R_2} + \dots + \frac{1}{R_n}. \quad (2.2)$$

Series resistors are treated as the sum of individual resistances,

$$R_{eq} = R_1 + R_2 + \dots + R_n. \quad (2.3)$$

In practical application, resistors are susceptible to series induction and parallel

capacitance in alternating current (AC) systems. These vulnerabilities are expressed primarily in the high frequency regime, which can impact signal amplification. Resistors are thermally emissive as a property of power dissipation. Power dissipation in an ideal resistor is modeled as

$$P = \frac{V^2}{R} = I^2R = IV. \quad (2.4)$$

This power is converted to heat and emitted by the component.

## Capacitor

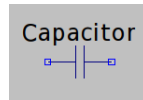


Figure 2-2: The symbol used to represent a capacitor in circuit diagrams.

A capacitor is a passive, two terminal component that stores electrical charge. When a voltage potential is passed along a capacitor, an electrical charge is produced. A capacitor consists of two charged conducting nodes separated by a non-conductive medium. This medium consists of either a vacuum or a dielectric material, which can increase the capacitance of the component. Capacitors are characterized by their capacitance. In an ideal capacitor, its capacitance is measured as the ratio of charge held to the voltage across the component. This is represented in the formula

$$C = \frac{Q}{V} \quad (2.5)$$

in a DC system. In AC systems, a capacitor's impedance influences the capacitance of the system. Impedance can be considered as a vector quantity described as the sum of the resistance and reactance, which is the component's opposition to current. Impedance is inversely related to capacitance and signal frequency.

The characteristics of capacitors in parallel and series are exactly opposite of a resistor. The capacitance of multiple capacitors in parallel are be calculated as the

sum of the capacitance of the individual components. This is represented by the equation

$$C_{eq} = C_1 + C_2 + \dots + C_n. \quad (2.6)$$

For capacitors in series, the total capacitance can be calculated as the multiplicative inverse of the sum of the reciprocals of individual resistors and represented by the formula

$$\frac{1}{C_{eq}} = \frac{1}{C_1} + \frac{1}{C_2} + \dots + \frac{1}{C_n}. \quad (2.7)$$

## Diode

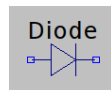


Figure 2-3: The symbol used to represent a diode in circuit diagrams. The positive terminal is to the left, and the negative terminal is on the right.

A diode is a unidirectional conductor that passes current from a positive to negative terminal, and restricts current flow in the reverse direction. A typical diode utilizes a p-n junction material to generate a forward direction with zero resistance, and a backward direction of infinite resistance. A diode has two response modes known as reverse-bias and forward-bias. A diode that is reverse-biased will act as an insulator and will ideally prohibit current from being passed, so long as its voltage limit is not exceeded. Conversely, a diode that is operating with a forward-bias will become a conductor, and current can pass backwards through the diode. Diodes also possess a property known as breakdown voltage, which flips a diode's bias when reached. When a diode is exposed to its breakdown voltage in the direction opposite the flow of current, the formerly infinite resistance drops to low resistance, and current backflows. This property is exploited to direct current in anomalous situations such as overvoltage. When an overvoltage situation occurs, a diode will switch from being negative-biased to being positively-biased, and will direct current away from sensitive components. Additionally, diodes have a characteristic voltage drop in the



direction of current flow, which is described in its commercial datasheet. This can be used to help shape a voltage in signal processing.

## Gain

In analog amplification systems like the SXM, gain refers to the ratio of output to input signal. Voltage gain will be primarily discussed henceforth, as this is what occurs in the SXM amplification chain, although power, amplitude, and current are all other methods of measuring gain.

### 2.1.2 Operational Amplifiers

An Operational Amplifier, or op-amp is a high-gain voltage amplifier that takes a differential input and produces a single output. It is directly coupled, meaning that it relies on direct current transmission, rather than through inductive or capacitive coupling [2]. In a circuit diagram, an op-amp has five terminals, which are labeled in Figure 2-4.

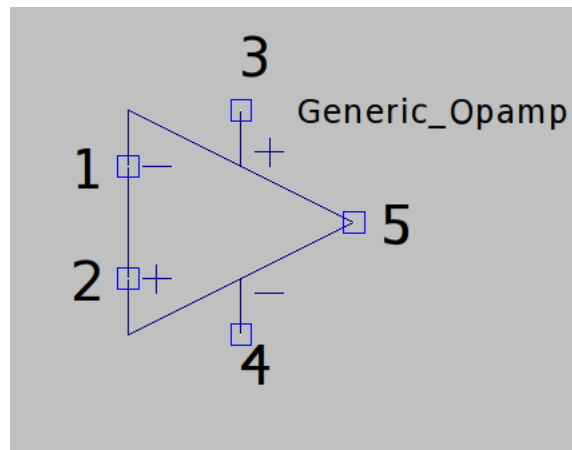


Figure 2-4: A generic op-amp. (1) Inverting input, (2) Non-inverting input, (3) Positive power supply, (4) Negative power supply, (5) Output.

Additionally, an ideal op-amp has the following characteristics [2]:

- No output impedance
- No noise contribution to the output signal

- No DC offset in the output signal
- Infinite bandwidth
- Infinite input impedance
- Infinite open-loop voltage gain

Open-loop gain is entirely dependent on the input. Consider Figure 2-5 in which an op-amp is placed in the open-loop configuration. For any non-zero voltage input, the open-loop gain drives the op-amp output into saturation. When the op-amp is saturated, the output voltage no longer increases. When the voltage input to the op-amp is zero, the output from the op-amp is also zero. An op-amp in the open-loop configuration is liable to latch-up, where the op-amp experiences a short circuit and ceases to work. Op-amp saturation is not always reversible, and can permanently disrupt current flow through the circuit.

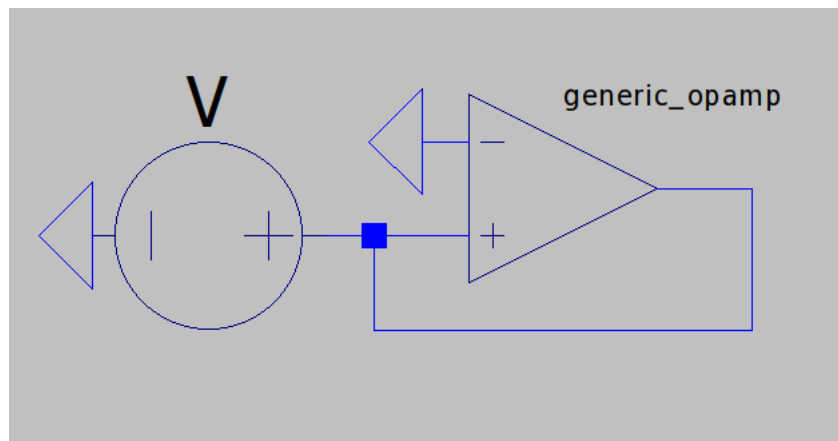


Figure 2-5: A generic op-amp with open-loop gain.

In order to guard against voltage output saturation, an op-amp can be configured for closed-loop gain, as shown in Figure 2-6. Closed-loop gain relies on the output signal feeding back into the input in order to shape desired input. Op-amps that amplify through the use of closed-loop gain are less susceptible to voltage saturation through amplification. However, it should be noted that saturation can still occur through overvoltage from the input.

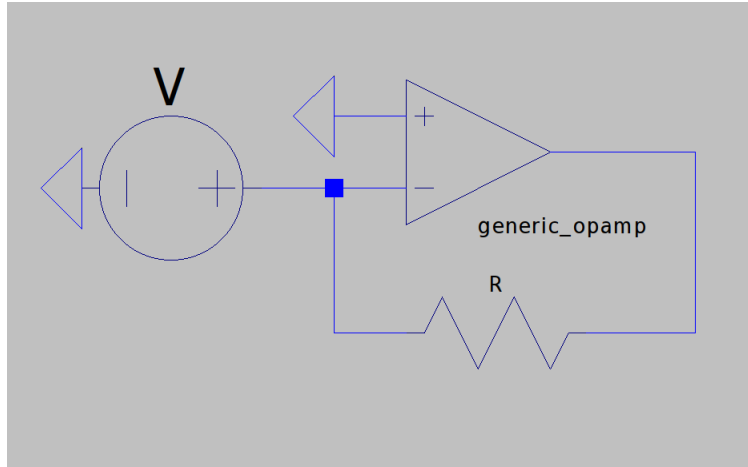


Figure 2-6: A generic op-amp with closed-loop gain.

### 2.1.3 Signal Amplification

The SXM uses a signal amplification chain to shape and condition x-ray flux signal for analog-to-digital conversion. Two different input configurations will be discussed in this section, and select common amplification circuits will be explained.

Inverting amplifiers take a positive DC voltage at the input and produce a larger negative voltage at the output. In AC amplification, the output is exactly  $180^\circ$  out of phase with the input. Non-inverting amplifiers take an AC input and preserve its phase in the amplified output. A positive voltage DC input will yield a positive voltage output.

The first common amplification circuit is a differentiator, shown in Figure 2-7. A differentiator is created using an inverting amplifier with a capacitor in the input line, and a resistor in the negative feedback loop, which can be considered a rudimentary high-pass filter. This causes the output from the op-amp to be proportional to the time derivative of the input, which is where the circuit owes its name. The differentiator has a few characteristic limitations. For instance, a differentiator is susceptible to circuit noise which may be amplified in the output. A differentiator is also susceptible to high-frequency noise, which can cause instability [2].

Similar to the differentiator, an integrator is used to integrate and invert an input signal. The output voltage is the time-dependent integral of the input voltage [2]. In

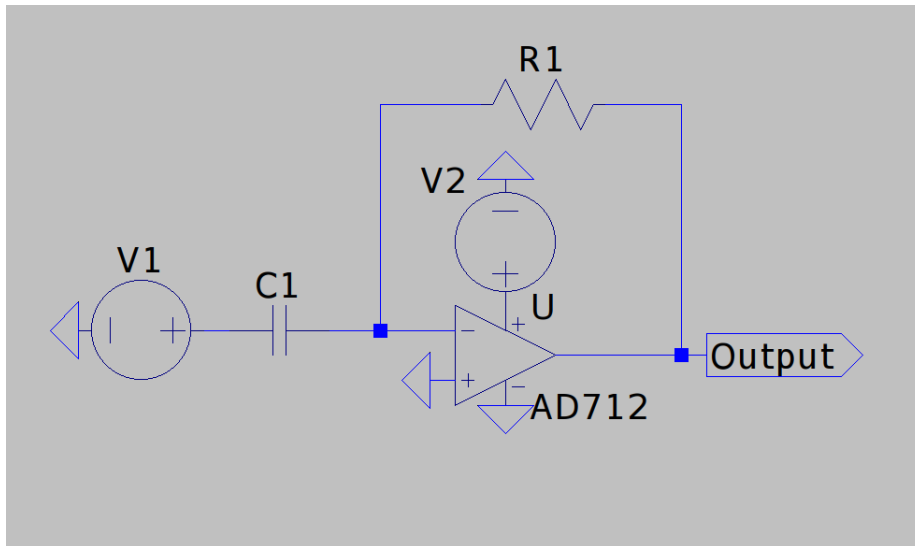


Figure 2-7: An example differentiator circuit.

this configuration, a resistor is included on the input line, and a capacitor is placed in the negative feedback loop, which creates a low-pass filter, as shown in Figure 2-8.

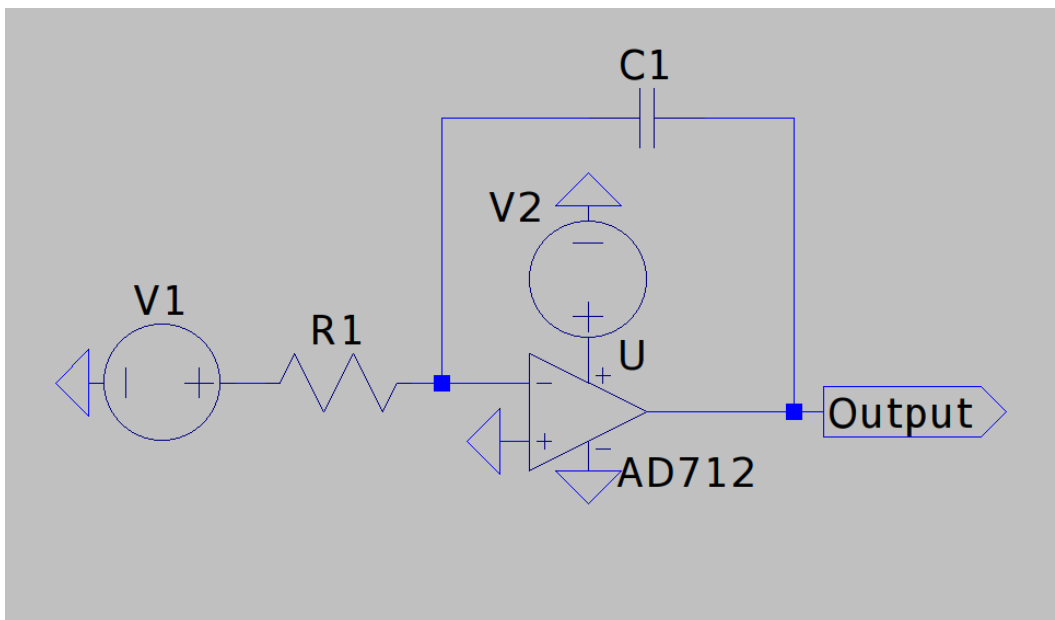


Figure 2-8: An example integrator circuit.

In its simplest configuration, an integrator circuit requires periodic discharge of the capacitor, which can become saturated with charge. When this occurs, the output voltage can drift beyond the optimal range of the op-amp. One way to mitigate this

challenge is to include a resistor in the feedback loop that functions as a discharge path for the loop capacitor (Figure 2-9).

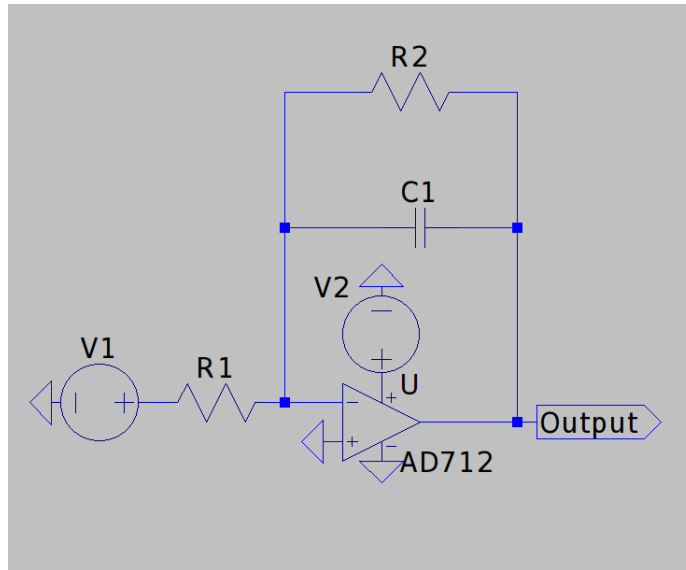


Figure 2-9: An integrator circuit with an additional resistor added to the feedback loop provides a discharge path for the capacitor.

The last configuration worth mentioning is the Schmitt Trigger, which shapes an input signal into a square wave. An example Schmitt Trigger is provided in Figure 2-10. This configuration can be used to shape a signal at a set voltage, so that it can achieve a more lossless input into an analog-to-digital converter. A Schmitt Trigger is a modified integrator with positive feedback. A voltage divider is used to set the positive feedback, and looped back to the non-inverting input. When a prescribed threshold voltage is exceeded, the input voltage triggers and changes the state of the output voltage. This configuration is vulnerable to hysteresis effects, where the input voltage is above the threshold voltage.

#### 2.1.4 Analog-to-Digital Signal Conversion

Analog-to-digital conversion is the process through which an analog signal is translated into a series of digital values using an analog-to-digital converter (ADC). In the SXM, an input x-ray signal is amplified and shaped before being converted and digitized for data processing. The digital output from the ADC is proportional to the

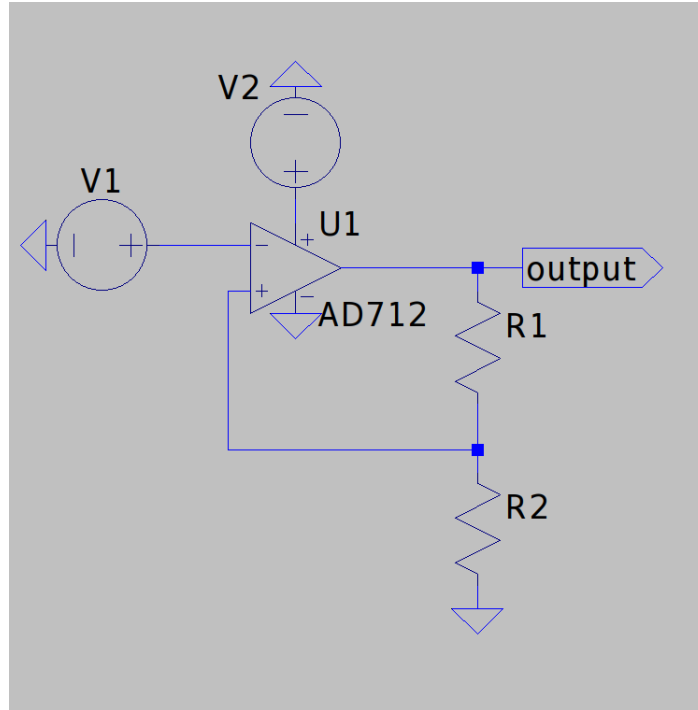


Figure 2-10: An example Schmitt Trigger.

analog input signal, and is limited by quantization speed and accuracy concerns.

### 2.1.5 Thermal Impact on Circuitry

Temperature concerns must be accounted for when creating and operating complex electrical systems. Amplification circuits often have a small window of acceptable input voltages, and signals must remain within specified bounds in order to be amplified and ultimately converted by an ADC. Furthermore, unwanted over- or under-voltage can cause temporary or even irreversible damage to sensitive electrical systems.

While voltage itself is not thermally dependent, individual circuit elements are dependent. For instance, an increase in temperature can affect power dissipation in resistors. This can cause permanent damage to resistors by burning or melting the resistor. In capacitors, temperature can alter how charge moves within a dielectric material, increasing or decreasing the amount of charge required to saturate the component. Additionally, resistivity in the wiring connecting circuit elements scales positively with temperature, which can cause unintended voltages within the circuit.

Temperature concerns are considered in the design process of space hardware. For Class D missions, NASA recommends that only Level 1, Qualified Manufacturer List Class V (QMLV) legacy hardware is used in instrumentation. Circuitry tested to this level is rated for interplanetary spaceflight, where extreme radiation and thermal conditions are experienced [10].

## 2.2 SXM Overview

The SXM component of the REXIS instrument suite is a subassembly located on the OSIRIS-REx bus such that it will face the sun during windows of operation that REXIS is pointed at Bennu. The electrical elements of the SXM are attached to the REXIS Main Electronics Board (MEB) by a coax tether. The SXM mechanically adheres to the spacecraft bus using an aluminum mounting bracket. The external elements of the SXM consist of an Amptek XR-100SSD silicon drift diode (SSD) detector connected to a pre-amplification circuit (henceforth referred to as the preamp) located on a mounted printed circuit board (PCB).

When a solar x-ray hits the SSD detector, an analog signal is passed through the preamp, where it is conditioned and sent to the MEB. At the MEB, the analog signal passes through an ADC, which outputs a digital response. This digital response is processed further by the MEB into x-ray energy event histograms sorted by energy level. Event energy data is kept in Analog-to-Digital Units, which can be converted to units of Electronvolt (eV). A conversion from ADU to eV is calculated using the formula

$$keV = 0.0219 * ADU, \tag{2.8}$$

for the REXIS SXM.

Solar x-rays and their energies are then used to calculate the influx and energy of primary solar x-rays onto Bennu. A knowledge of primary x-ray energies is required to calibrate the secondary x-ray fluorescence capture by the REXIS detector.

## 2.3 SXM Data Pipeline

The SXM Data Pipeline takes a converted signal from the SXM ADC and processes it into data packets that are transmitted to the ground.

### 2.3.1 Instrument Response Modeling

The SXM underwent a series of ground and in-flight validations between 2013 and 2019. This section will focus on the instrument response modeling that was used to verify early in-flight observations. The SXM Data Pipeline included a model of ideal SXM response, which at its core took a sample time-series of x-ray detections and produced energy histograms. These energy histograms could then be fitted to a known solar abundance model, which would match an input signal to x-ray characteristics of elements in the Sun's photosphere, and subsequently constrain solar temperature at the time of x-ray emission. While this function fell beyond the original scope of the SXM's purpose, it provided yet another way to produce instrument science.

### 2.3.2 Chianti Atomic Database

The Chianti Atomic Database was used to create an instrument response model across all temperatures and energies observable by the SXM. The Chianti Database is an atomic spectra database built and maintained by a global consortium of atomic scientists [8]. Chianti and its associated python package, ChiantiPy, allow a user to generate model spectra of astrophysical bodies. For the purposes of the SXM, Chianti provided a known database against which sample SXM histograms could be matched. Both coronal and photospheric abundance models were generated at the temperatures and energies observable by the SXM, and ideal instrument response was cross-referenced against early in-flight calibration data that was taken prior to the REXIS instrument's primary observation window. The intention of this cross-reference was to build reasonable confidence in the instrument response model such that temperatures and spectra abundances could be derived from data collected during observation.



# Chapter 3

## SXM Design and Operation

This chapter describes the design process and flight operations of the REXIS Solar X-ray Monitor (SXM). The first section will focus on the design constraints of the instrument. REXIS is a Risk Class D mission, which means it is a low budget instrument, and is designed to use legacy, off-the-shelf components [11],[12]. This section also describes the science mission requirements for the SXM, as well as design requirements stipulated by the OSIRIS-REx team. The design section will primarily detail the development of the SXM signal amplification chain, which is at the center of the Root Cause investigation found in Chapter 4.

The next section of this chapter will describe the testing battery used to characterize the SXM on the ground and in flight. The SXM's pre-flight ground testing regimen will include testing data relevant to the SXM root cause analysis, and include rationale for why some tests were foregone. Results of SXM flight testing will be presented, and nominal x-ray count data will be shown.

The last section of this chapter summarizes SXM flight operations. A timeline of operations is included to understand where flight testing occurred relative to science observations. Flight operations are separated into three distinct phases, which correlate to OSIRIS-REx mission phases. Early flight operations are described, followed by operations during Orbital B and Orbital R, the SXM's two science operation phases.

## 3.1 SXM Design Background

The SXM was first designed as part of the 16.83 undergraduate capstone class in the MIT Department of Aeronautics and Astronautics in 2011. This first design became the foundation upon which the SXM flight model was developed. The REXIS instrument was designed to use heritage spaceflight technology to reduce the design timeline. The SXM detector is an Amptek XR-100SDD, which is an updated model of detectors flown on previous x-ray instruments. The XR-100SDD is an updated version of the XR-100CR, and the former uses a silicon drift diode, while the latter uses a PIN photodiode [1]. Both models a beryllium window above an evacuated chamber in which the detector is housed. Amptek XR-100CR detectors were used in the Solar X-ray Spectrometer aboard GSAT-2, a space-based Indian solar observatory [5]. A similar Russian space observatory used the XR-100CR in the Solar Photometer in X-rays (SphinX) instrument [15]. Both of these previous instruments demonstrated that the Amptek XR-100 class detector could be reasonably be used to for x-ray solar observation, despite the XR-100SDD never having flown prior to REXIS.

The XR-100SDD detector was also included in early designs of the Neutron star Interior Composition ExploreR (NICER) instrument. NICER was developed by the MIT Kavli Institute (MKI), and the engineering teams worked closely together in the development processes. Both Professor Richard Binzel and Dr. Rebecca Masterson, who represent two-thirds of REXIS leadership, are affiliated with the Kavli Institute. Additionally, the Kavli Institute is located in the same building as the REXIS team, meaning collaboration was as easy as going upstairs. Additionally, the Goddard Spaceflight Center serves as the managing center for both REXIS and NICER. This closeness of personnel was reflected in the design of the REXIS SXM.

The NICER instrument is mounted aboard the International Space Station, where its main spectrometer observes neutron stars in the 0.2 to 12 keV range [4]. The REXIS SXM shares both structural and electronic heritage with the NICER instrument. An early design of NICER implemented 56 XR-100SDD detectors, the same detector used by the REXIS SXM. The NICER team later changed their design to

use an Amptek CMOS detector, which benefits from higher temporal resolution.

While the NICER instrument and the REXIS SXM's designs diverged during the design phase, the SXM was heavily influenced by this early NICER design. The design of the SXM preamp circuit and SXM Electronics Board resemble the NICER preamplifier board and surrounding electronics housing respectively. These similarities are the legacy of John Doty, an engineer affiliated with MIT who created the SXM timing circuitry, signal pulse shaping, and threshold trigger. A complete documentation of SXM circuit diagrams can be found in Appendix A.

### 3.1.1 Mission Requirements

REXIS SXM requirements fall under the REXIS instrument's main requirements, which in turn are derived from OSIRIS-REx requirements for the instrument. The REXIS requirements documentation flow was described extensively in Mike Jones's Master's thesis [6]. The information flow diagram for REXIS is shown in Figure 3-1

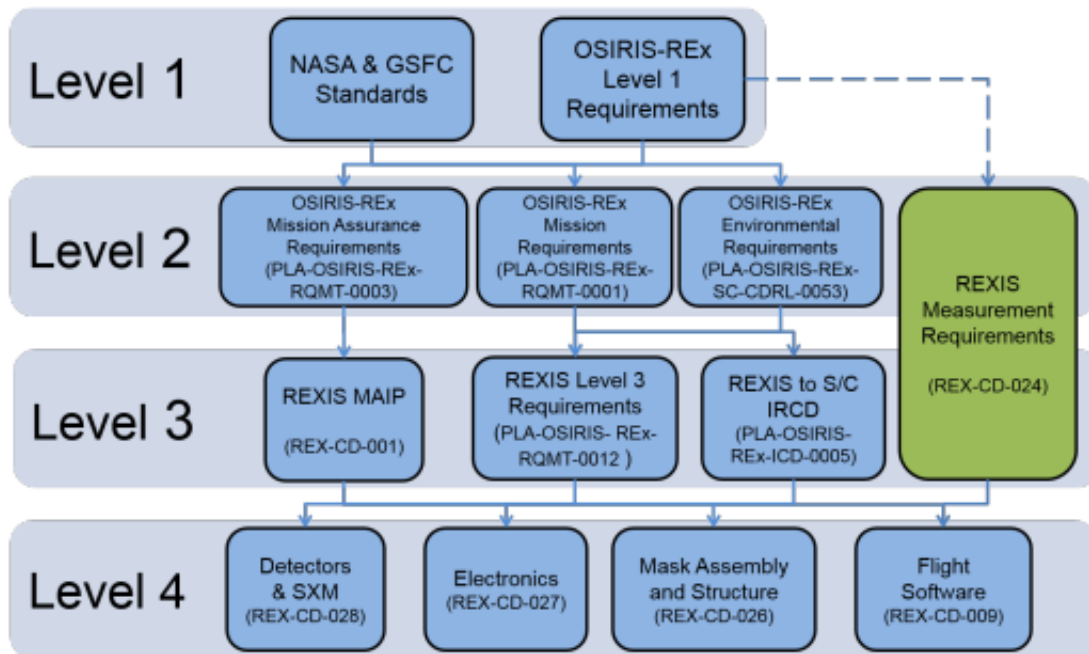


Figure 3-1: The REXIS Requirements documentation flow from Jones, 2015 [6].

The SXM's energy band of interest is from 0.6 keV to 6 keV. Quantum efficiency for the SXM is also outlined in the REX-74 requirement. Quantum efficiency is the

ratio of photon events that are successfully converted to electrons by the detector, and is a metric used to evaluate the performance of an instrument at different detection energies (shown in Table 3.1).

Quantum Efficiency	Energy Range (keV)
>0.01	0.62 - 0.7
>0.03	0.7 - 0.8
>0.09	0.8 - 1.2
>0.65	1.6 - 2.8
>0.85	2.8 - 4.1
>0.9	6.0 - 7.0

Table 3.1: Quantum Efficiency Requirements for the SXM Detector.

The REXIS SXM Requirements are derived from the different levels of REXIS requirements. SXM operational and environmental requirements are found in the Level 4 documentation. Level 3 documentation describes the requirements for detector functionality. The Level 2 requirement REX-7 is the highest-level requirement pertaining to the SXM. REX-7 requires that the SXM "shall measure solar coronal temperature to within 0.1 MK every 50 sec while observing Bennu in Phase 5B assuming a single temperature model." A complete overview of Level 3 and Level 4 requirements can be seen in Tables 3.2 and 3.3.

ID No.	Title	Description
REX-225	Integration Time	The SXM shall integrate counts for 32 seconds (nominally) to form a spectrum.
REX-73	Spectral Resolution	The SXM shall have a spectral resolution (FWHM) that is less than 200 eV from 0.6 to 6 keV.
REX-74	Quantum Efficiency	The SXM shall detect x-ray events from 0.6 to 6.0 keV with quantum efficiencies as given in Table 3.1.
REX-75	Field of View	The SXM shall have a full width zero intensity (FWZI) FOV of no greater than 60 deg full cone and a full width full intensity (FWFI) FOV of no less than 10 deg full cone.

Table 3.2: SXM Level 3 Requirements.

ID No.	Title	Description
REX-228	SDD Survival Temperature	The temperature of the SDD shall always be greater than $-65^{\circ}\text{C}$ and less than $150^{\circ}\text{C}$ .
REX-229	SDD Operating Temperature	The temperature of the SDD shall be less than $-30^{\circ}\text{C}$ and greater than $-70^{\circ}\text{C}$ .
REX-76	Preamp Survival Temperature	The temperature of the SXM Preamp shall be greater than $-55^{\circ}\text{C}$ and less than $85^{\circ}\text{C}$ .
REX-77	Preamp Operating Temperature	The temperature of the SXM preamp shall be greater than $-40^{\circ}\text{C}$ and less than $85^{\circ}\text{C}$ while operating.
REX-78	SXM Health	The SXM shall survive and remain operational through the end of Phase 8.
REX-79	SXM Operational Time	The SXM shall be capable of operating 24 hours per day

Table 3.3: SXM Level 4 Requirements.

### 3.1.2 Overview of SXM Signal Amplification Chain

The SXM amplification chain is responsible for priming a signal from the SDD detector before it is converted by the Analog-to-Digital Converter (ADC). The amplification chain is housed on the SXM Main Electronics Board (MEB), which is located within the REXIS instrument on the spacecraft. The SXM detector and preamp circuit are housed in the SXM backpack, which is bolted to the outside of the spacecraft, and is connected to the MEB by a coaxial cable. The SXM detector housing is shown in Figure 3-2.

The SXM ADC requires a positive voltage signal pulse to be passed to it in order to register a detection count. When an x-ray strikes the detector, an analog signal pulse is created. The raw signal biased at 3.3 V, sent through the preamp, and then sent across the coax cable to the MEB. When the signal reaches the MEB, it is passed through three opamps, which amplify the signal. Then the voltage signal is divided, where one signal passes through an integrator circuit and the other signal through a differentiator circuit. The output from the integrator circuit is labeled *outu*, and the output from the differentiator circuit is labeled *outb*. The amplification chain schematic diagram is shown in Figure 3-3. Additional SXM electronics schematics

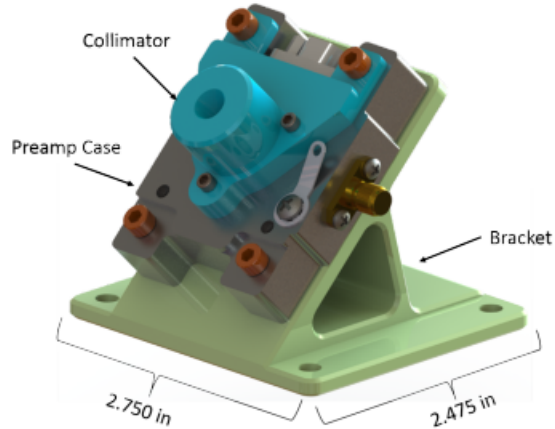


Figure 3-2: SXM detector and preamp housing. The SXM detector is located below the collimator.

can be found in Appendix A.

The signals are then sent through a low pass filter to eliminate high frequency noise artifacts added to the signal when it passed through the preamp circuit. The *outu* signal is then sent to the final section of the amplification circuit, where 3 V of bias are subtracted, leaving the signal with a residual 0.3 V bias. This bias is required to keep the *outu* signal positive because the ADC used in the SXM electronics chain is not rated for negative voltage inputs.

Next, Signal *outu* is sent to the ADC to be measured, while signal *outb* is sent to a zero cross monitor, which provides the timing for the ADC to sample new signal, now named *outu1*.

In order to trigger an ADC detection, the SXM relies on a trigger circuit that uses a series of comparators to compare *outb* to a reference voltage. The trigger circuit is shown in Figure 3-4.

This trigger includes a command to manually set the threshold Voltage Lower Limit of Detection (VLLD). The VLLD is set above the *outb* bias voltage as well as the noise floor to prevent the SXM from accidentally triggering due to random noise in the electronics. The relationship of *outb* to VLLD is given as:

$$LLD = outb - VLLD, \quad (3.1)$$

SOLAR X-RAY MONITOR SHAPING AND AMPLIFICATION

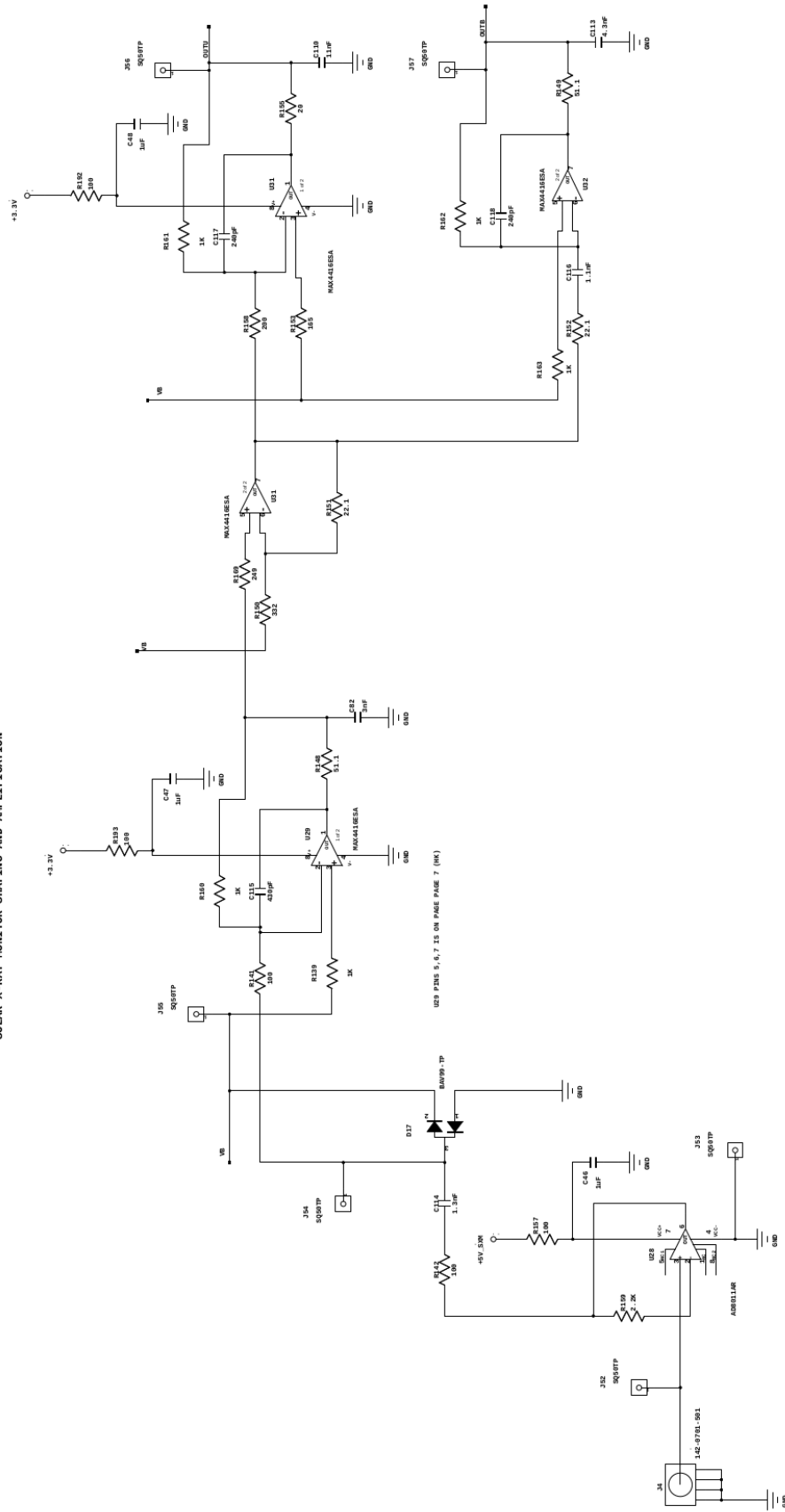


Figure 3-3: Schematic of SXM Amplification Chain. Outputs *outb* and *outu* are seen on the far right.

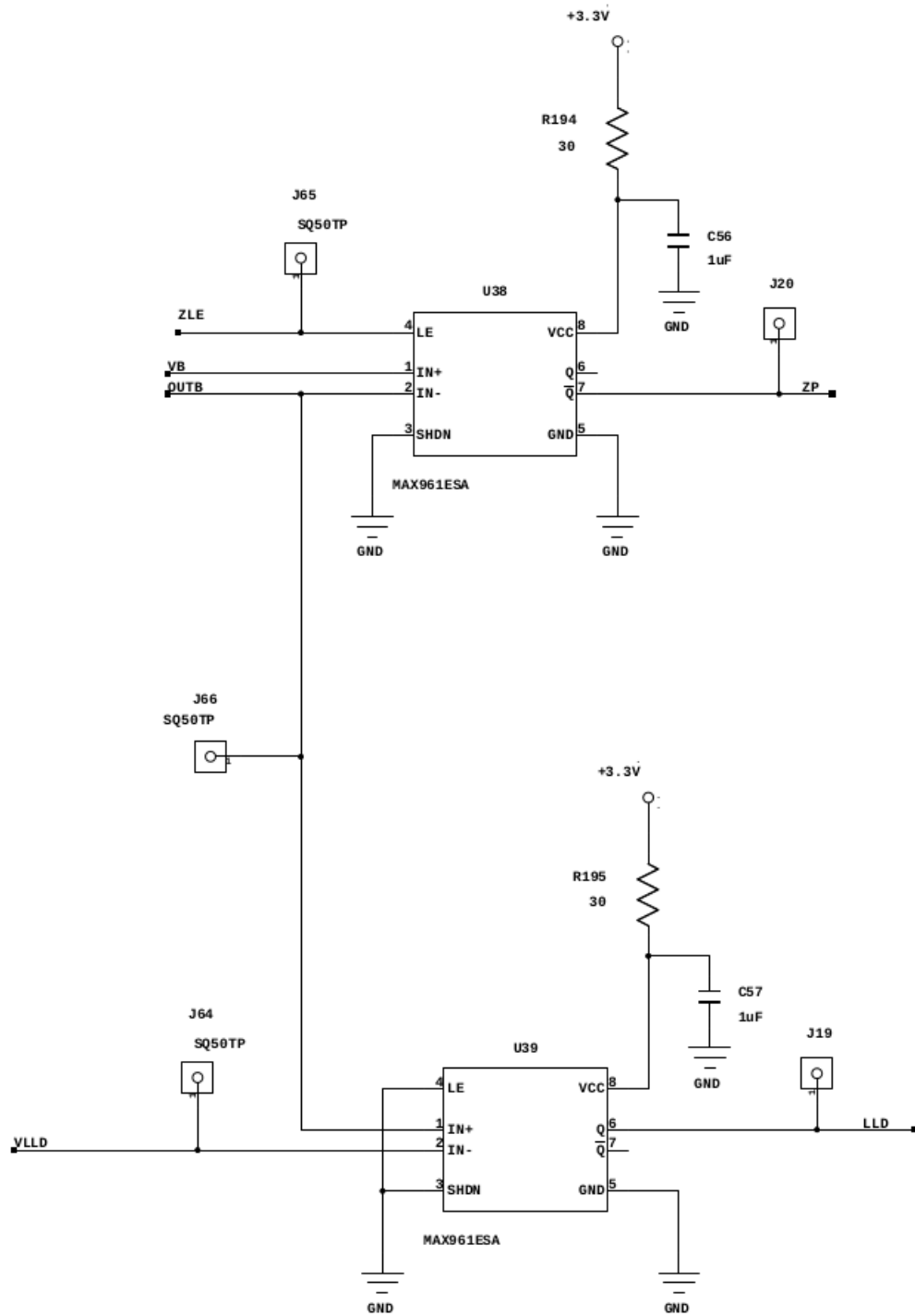


Figure 3-4: SXM Trigger Circuit Schematic.

where LLD is the Lower Limit of Detection. A threshold setting anomaly was discovered early in flight, where the threshold would fluctuate. This was resolved by sending



three threshold setting commands to the instrument. The first two commands were to set the threshold to an arbitrarily high value, and the third command was to set the threshold to the intended value. This workaround was only used once, but resolved noticeable threshold drift for the remainder of flight.

The second threshold circuit is used to determine the zero crossing of *outb*. When *outu1* is at it's peak, *outb* will have a zero crossing, and the ADC is triggered to begin recording. Figure 3-5 shows an example of all signal shapes.

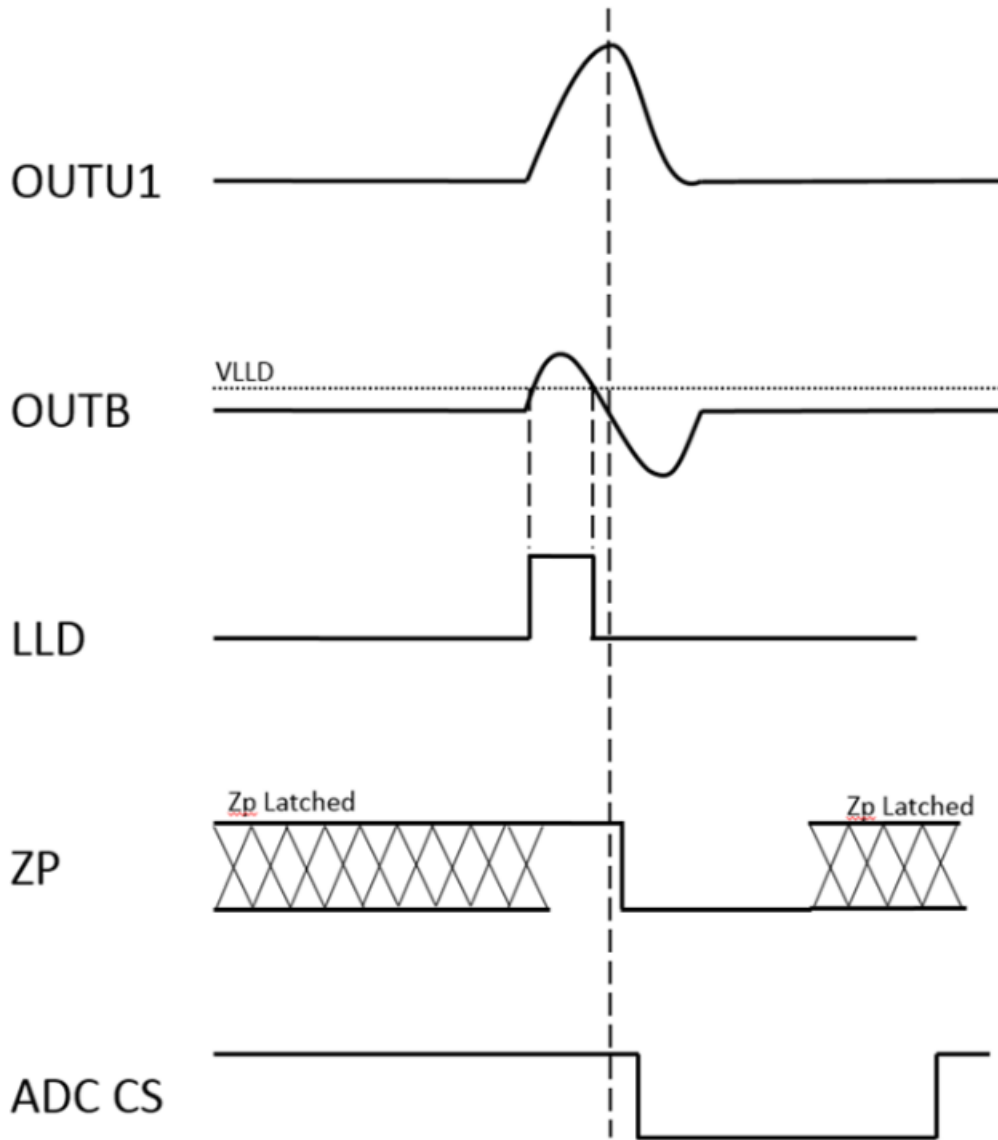


Figure 3-5: SXM signals at various points throughout the amplification chain.

## 3.2 Instrument Testing

As part of the instrument design process, the REXIS SXM was subject to numerous functionality tests on the ground. Testing was limited by time and financial constraints, but the testing framework was rigorous and proved the SXM ready for flight. The subsection on ground testing will focus on testing that aided in characterizing the SXM low count rate anomaly discussed in Chapter 4. A more thorough description of SXM ground testing can be found in Kevin Stout’s thesis [14].

The SXM also underwent a series of flight tests between launch in 2016 and Orbital B, the first data collection phase, in July of 2019. Flight testing was primarily used to characterize the REXIS main spectrometer, whose CCD array required in-flight calibration, although the SXM was tested as well [7].

### 3.2.1 Ground Testing

The SXM was put through a battery of ground tests to ensure the instrument was ready for flight testing. The testing procedure followed NASA requirements for Risk Class D missions [11]. The focus of this subsection will be on SXM thermal tests, which provided a background for the root cause analysis outlined in Chapter 4.

The SXM was subject to thermal testing using thermal vacuum chambers built in the MIT Space Systems Laboratory and at MIT Lincoln Laboratory.

#### **SXM Oven Test**

The SXM MEB underwent an oven test at Lincoln Laboratory in November of 2015. The complete SXM flight assembly, including the preamp and SDD detector, were placed in a thermal chamber. The MEB remained connected to the SXM assembly, but outside the chamber. The MEB was held at a temperature of approximately 20°C. The temperature of the thermal chamber was then fluctuated between -40°C and 60°C with a ground calibration iron source to measure instrument performance as a function of temperature. This was a more drastic temperature fluctuation than was expected in flight, and was used to identify thermal vulnerabilities in the SXM.

An example histogram from the ground calibration source is shown in Figure 3-6.

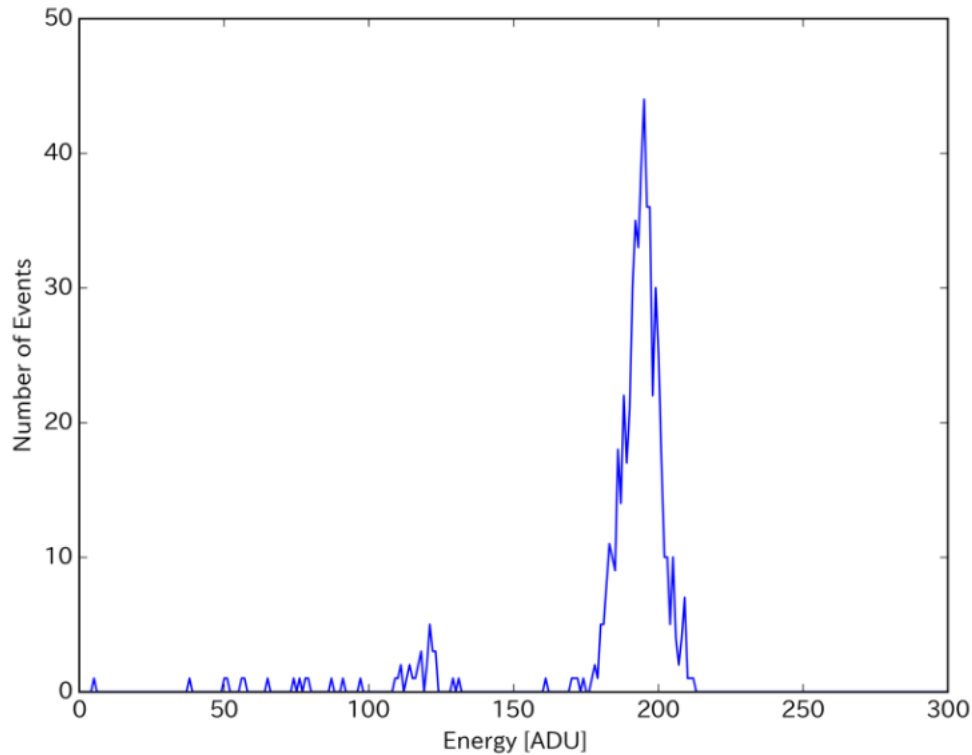


Figure 3-6: SXM Histogram of Ground Calibration Source. A strong iron line can be seen at around 200 ADU.

The preamp and SDD detector remained insensitive to temperature fluctuations over the test range. Additionally, it was discovered that both low and high energy artifacts set in at approximately 53°C. The results of this test are provided in Figure 3-7.

### **MEB Thermal Characterization**

The SXM MEB was included in a similar thermal test. The MEB was placed in the thermal test chamber, where its temperature was then cycled between -40°C and 60°C, while the SXM was exposed to the Fe-55 ground calibration source. Figure 3-8 shows temperature changes in the SXM during testing.

At high temperatures, the SXM recorded lower source counts than at lower temperatures. Hysteresis effects were also seen in the MEB, and it was determined that

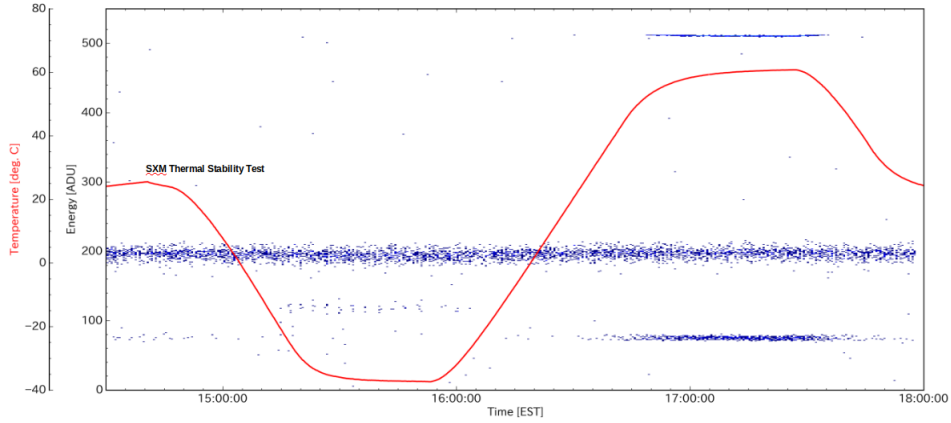


Figure 3-7: Results of SXM Oven Test, November 2015.

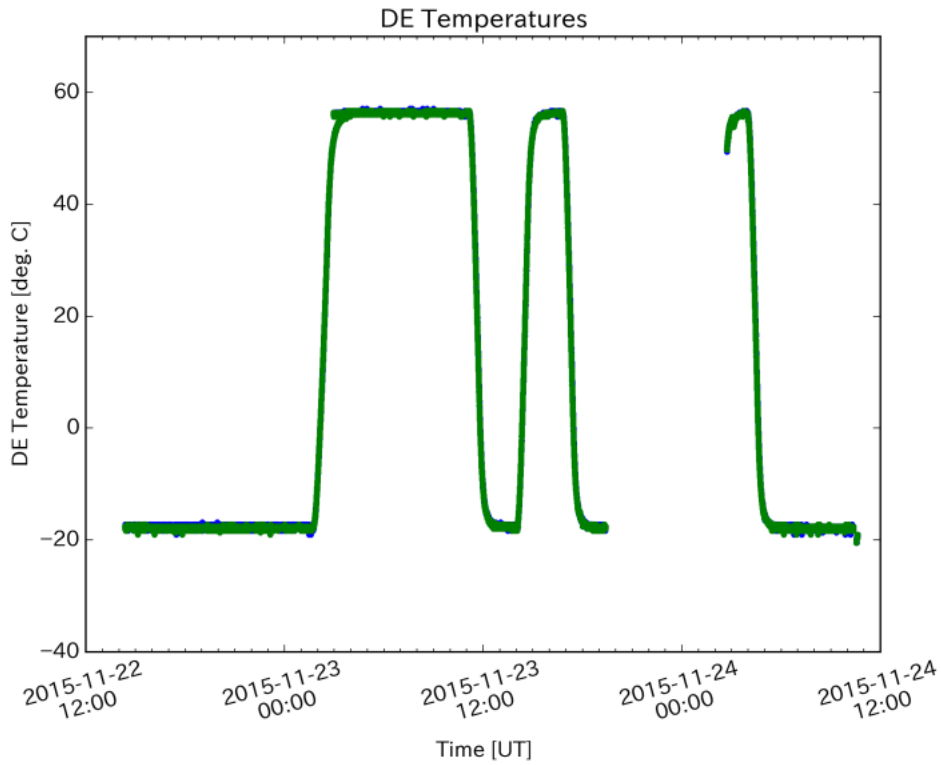


Figure 3-8: Temperature Fluctuations during the MEB Thermal Characterization Test.

temperature changes in the MEB can result in changes to the SXM's low energy threshold. The results of this test are provided in Figure 3-9.

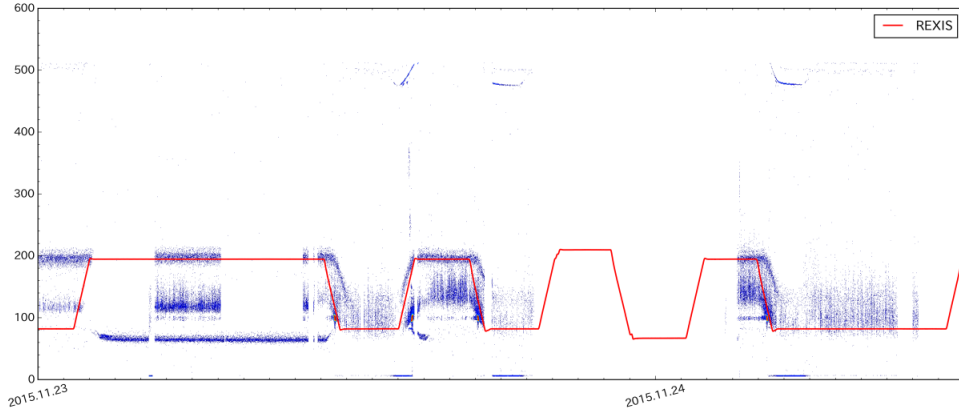


Figure 3-9: Ground Testing results of MEB susceptibility to temperature fluctuations.

### 3.3 Flight Operations

This section will describe the REXIS SXM during flight operations, from launch in September 2016 to planned shutdown in November 2019. The REXIS SXM operated over a period of approximately 3.5 years. The SXM was first powered on during L+14 days for a payload functions check. It was powered on at various times in flight during which it underwent calibration and additional functions checks. The SXM entered its first data collection phase in July, 2019 during Orbital B. Due to unanticipated low x-ray counts during Orbital B, it was powered on for an additional observation window in November, 2019 as part of the Orbital R mission phase.

#### 3.3.1 Early Flight Operations

Early flight operations for the SXM were characterized by a series of functionality tests, which served as milestones towards the ultimate goal of data collection during the Orbital B mission phase. The first of these calibrations occurred during the L+14 days payload check. The SXM collected 3935 seconds of nominal x-ray data, and the instrument was determined to be working properly.

The next notable evaluation of the SXM occurred during L+30, which took place in January, 2019. L+30 was the first time that Bennu was in the field of view of the REXIS main spectrometer, and was a critical functionality check for the instrument.

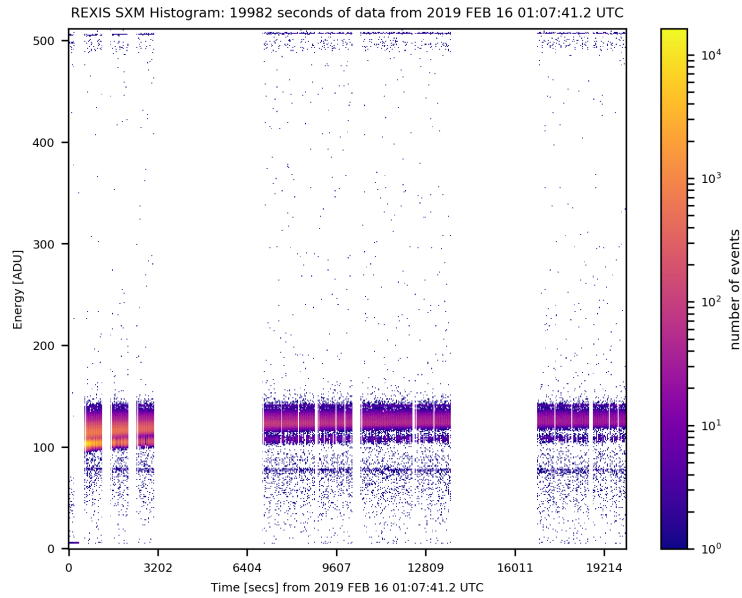
The L+30 mission phase was divided into two distinct flight patterns. The first had the REXIS main spectrometer pointing nadir at the asteroid, while the second had the main spectrometer pointing away from the asteroid. During the second phase of L+30, the SXM recorded a low x-ray count rate from the sun, which was because the instrument was not directly facing the sun, as it was during the first phase of L+30. A comparison of L+30 flight data are shown in Figure 3-10. This example of off-pointing low x-ray counts became an important comparison data set with which to compare Orbital B data.

### 3.3.2 Flight Operations during Orbital B

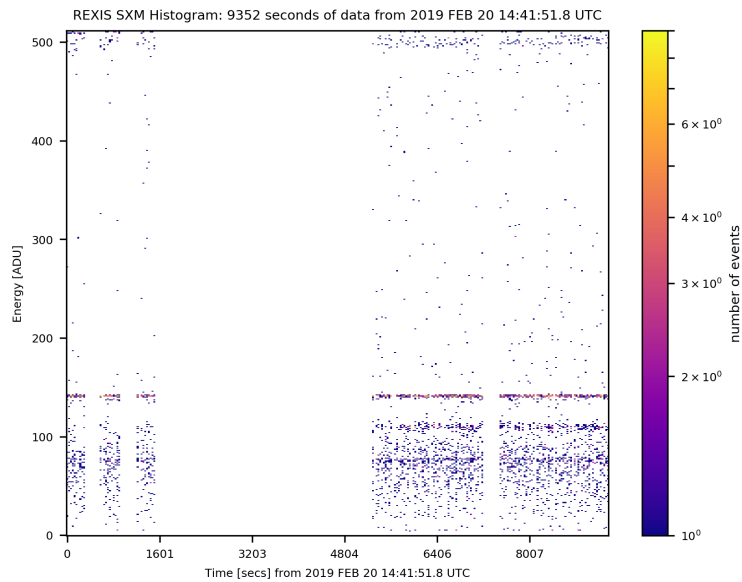
The SXM entered its primary data collection phase during Orbital B, which occurred in July, 2019. On 5 July, the SXM suffered a "bit flip" error, where each detection was saturated by an additional value of 34880. This was noticed when the daily histogram data was saturated at an extremely high count rate. The "bit flip" most likely occurred when the SXM was struck by a high energy cosmic ray, which shifted the reset value of the SXM from its minimum value to its maximum. This required a reset of the instrument from the ground, which reverted the SXM reset value to its designed minimum.

Once the "bit flip" had been resolved, the SXM remained operational for the rest of Orbital B. During Orbital B, the SXM recorded an x-ray count rate two orders of magnitude lower than what was previously seen during the first part of Internal Calibration. An example event rate histogram from Orbital B is shown in Figure 3-11.

Low x-ray counts persisted for the remainder of Orbital B, and were subsequently the focus of an anomaly report made to the OSIRIS-REx team. These low x-ray counts were unexpected, and highlighted anomalous performance in the instrument, give the spacecraft's heliocentric distance, and the solar state. While the Sun was recorded at a quiet A6.7 state, x-ray counts should have reflected a higher solar flux.



(a) Nadir Pointing REXIS Main Spectrometer



(b) Off-Point REXIS Main Spectrometer

Figure 3-10: SXM Event Rate Histograms during L+30

### 3.3.3 Flight Operations during Orbital R

The REXIS instrument team requested an additional observation due to lower than anticipated counts by the SXM and REXIS main spectrometer during Orbital B. The OSIRIS-REx mission operations team allowed the REXIS instrument to have an additional observation window during Orbital R, which took place during November

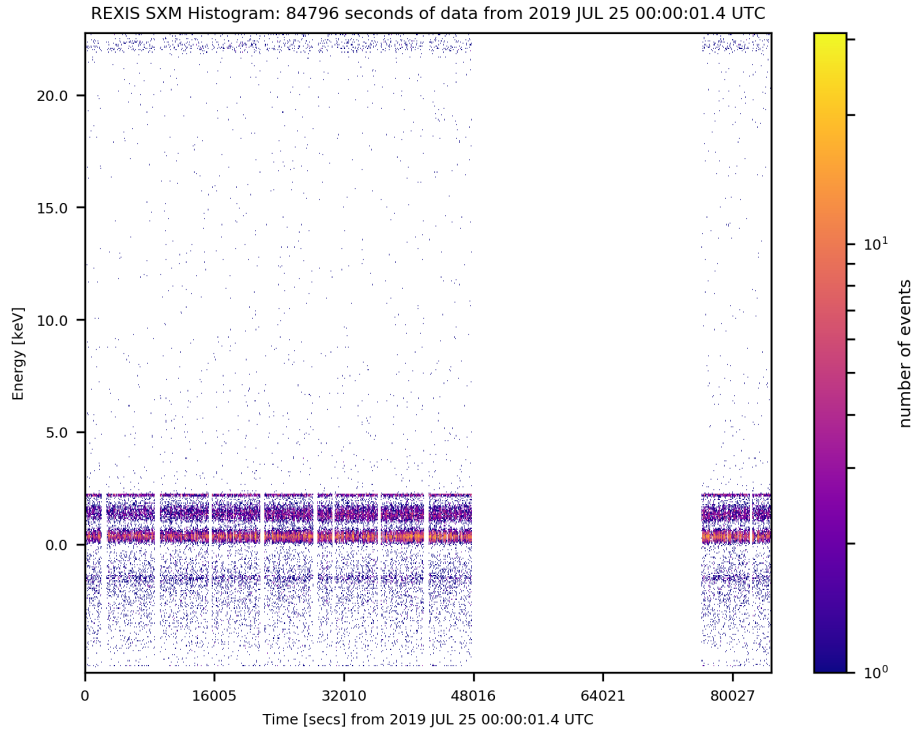


Figure 3-11: SXM Event Rate Histogram from Orbital B, 25 July 2019.

2019. It was hoped that when REXIS was powered on for Orbital R, the main spectrometer would detect higher flux counts from the asteroid, and the SXM would report x-ray counts at the expected rate.

During Orbital R, the SXM recorded low x-ray counts similar to those seen in Orbital B. An example Orbital R event rate histogram is shown in Figure 3-12.

As Orbital R progressed, the SXM event rate began to decline. This coincided with a change in temperature in the SXM MEB, which occurred on 18 November, 2019. The secondary count drop off occurred rapidly over the course of the day, and can be seen in Figure 4-4. The SXM recorded low counts for the remainder of Orbital R. An investigation of the cause of these low x-ray counts is described in Chapter 4.



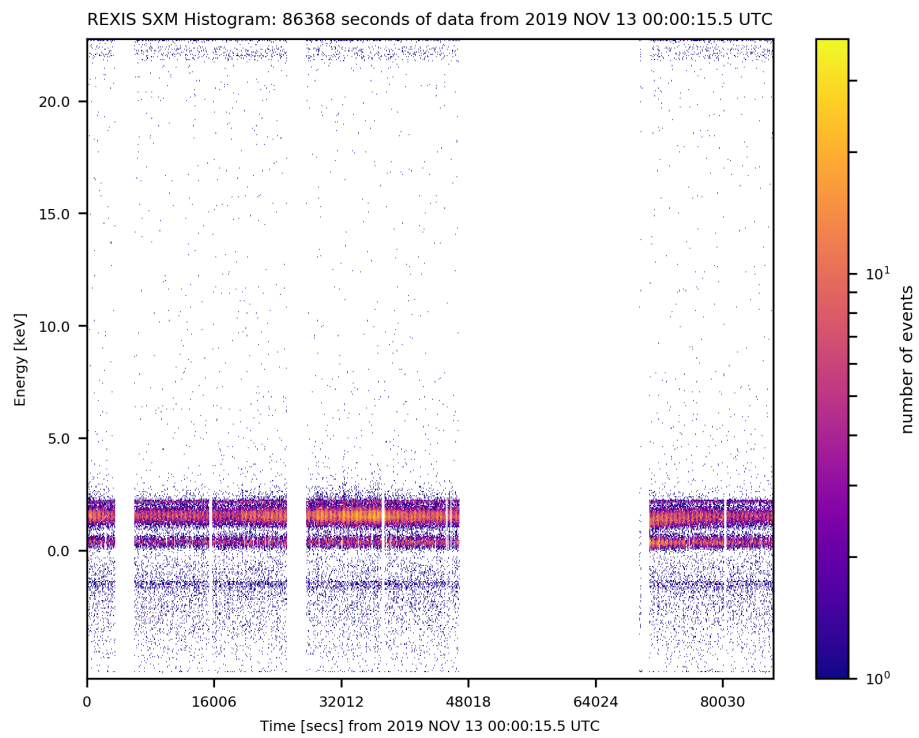


Figure 3-12: SXM Event Rate Histogram from Orbital R, 13 November 2019.



# Chapter 4

## SXM Root Cause Analysis

This chapter presents a preliminary root cause analysis of the SXM low count rate anomaly that began on 3 July, 2019, at the beginning of the Orbital B observation window. A root cause was chosen to examine the failure of the SXM as an instrument. It consists of an investigation into all possible causes of failure, which is the fourth probable cause described in a fishbone diagram (shown in Figure 4-1).

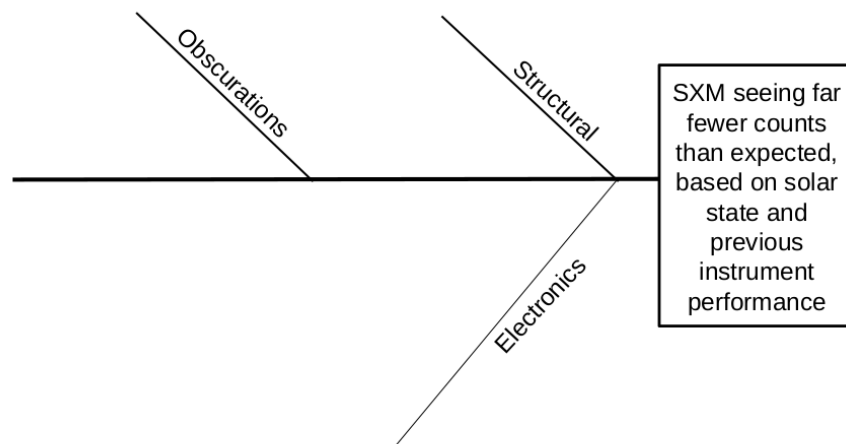


Figure 4-1: Example Fishbone diagram used to outline a Root Cause Analysis. Each bone is used to categorize the type of cause.

Based on evidence collected during a preliminary investigation by the instrument team, the most likely cause of low x-ray counts in the SXM was hypothesized to be due to a change in temperature in the signal amplification change. This thesis

will focus on the subsequent investigation of the thermal vulnerability of electronic components in the SXM. A brief explanation will be given for why other bones on the fishbone diagram have been discounted as the causes of failure.

In this chapter, an investigation report delivered to the OSIRIS-REx PI will be presented. A section will be devoted to how the anomaly was first identified, and the methods used to bound the problem. SXM response modeling to Orbital B data will be shown, and how it corresponds to deviations in the SXM's long-term temperature. LTSpice simulations show that modeling capabilities are limited by vendor simulation code, and leave a path forward for further research. A preliminary conclusion is offered, and a recommendation for future investigation is provided. As a point of reference, the terms "count rate" and "event rate" will be used interchangeably, as the SXM histogram data are recorded as counts (or particles striking the diode detector) per energy level, recorded in 32 second bins.

## **4.1 SXM Low Count Rate Anomaly**

The SXM received lower than expected counts during its two observation windows. This problem was first identified in Orbital B, and was subsequently observed in all of Orbital R as well. It was an ongoing impediment to solar science using the SXM, and its exact cause remains an open area of investigation.

### **4.1.1 Orbital B**

The SXM low count rate anomaly was first discovered during Orbital B, which took place in July and August of 2019. The SXM showed a decreased count rate that was atypical for the spacecraft's heliocentric distance. At this time, the spacecraft was located at a heliocentric distance of 1.3AU, and was showing a solar state of A6.7 as recorded by GOES15, a solar observatory located in Low Earth Orbit (LEO). An A6.7 solar state is relatively quiet from the sun, which at this time was near solar minimum, a period of low solar output. Orbital B data were two orders of magnitude lower when compared to signal data taken during Internal Calibration, during which

the spacecraft was at a comparable heliocentric distance. SXM data from Orbital R show a similar signal discrepancy, shown in Figure 4-2.

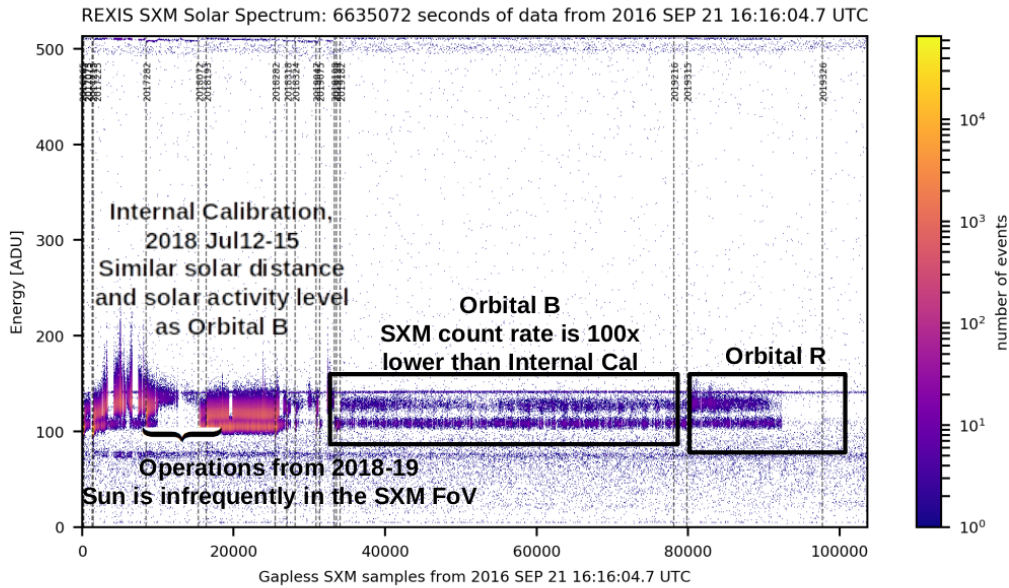


Figure 4-2: SXM count rate histogram from launch to Orbital R.

During Orbital B, the SXM also suffered an unrelated "bit flip" error, which caused each histogram bin to increase by a value of 34880. The bit flip was most likely caused by a strike from a stray high energy particle, which caused the 16-bit reset value to wrap around from 0 to 34880, the maximum value. This was first observed on 5 July, 2019, and resulted in a saturated event rate histogram. When this value was subtracted from these data, the corrected histogram showed values similar taken the previous day. A comparison of the saturated and corrected histogram is shown in Figure 4-3. The bit flip was corrected by manually resetting the histogram minimum value, which could be done from the ground. There were no issues with saturation in the SXM event rate for the remainder of Orbital B. The reset of the SXM offset did not impact the low count rate issue previously identified.

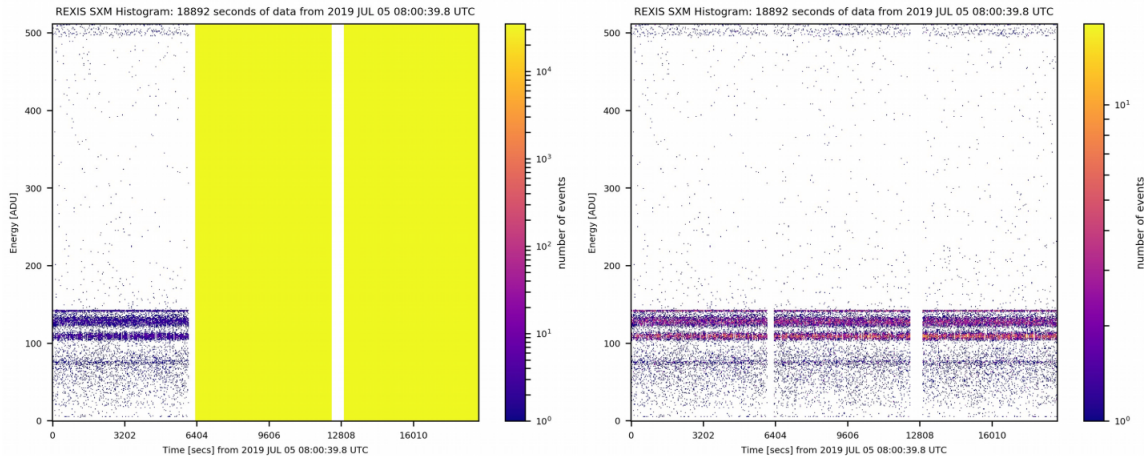


Figure 4-3: SXM Saturated Histogram (Right) and Corrected Histogram (Left)

### 4.1.2 Orbital R

Due to low counts during Orbital B, REXIS was allotted an additional 15 day observation window during November, 2019. On 18 November, 2019, SXM signal during Orbital R decreased beyond the low count rate seen in Orbital B, which can be seen in Figure 4-4. This decrease in signal is distinct from the previous six days observation in Orbital R, and demonstrates a departure from the previous low-count issue. This second decrease in signal persisted for the remaining 7 days of Orbital R.

A notice was provided to the OSIRIS-REx PI following the first instance of a lower than anticipated count rate during Orbital B. A subsequent incident, surprise, anomaly report (ISA) was requested, which was the formal directive for a root cause analysis into the instrument anomaly.

## 4.2 Constraining the Problem

Once the low count-rate anomaly had been identified, it became necessary to provide boundaries on the investigation. The following section begins with an overview of the ISA report and provides a fishbone diagram of the five likely root causes, as well as the rationale behind selecting thermal variability in the SXM Main Electronics Board (MEB) amplification chain as the most likely root cause.

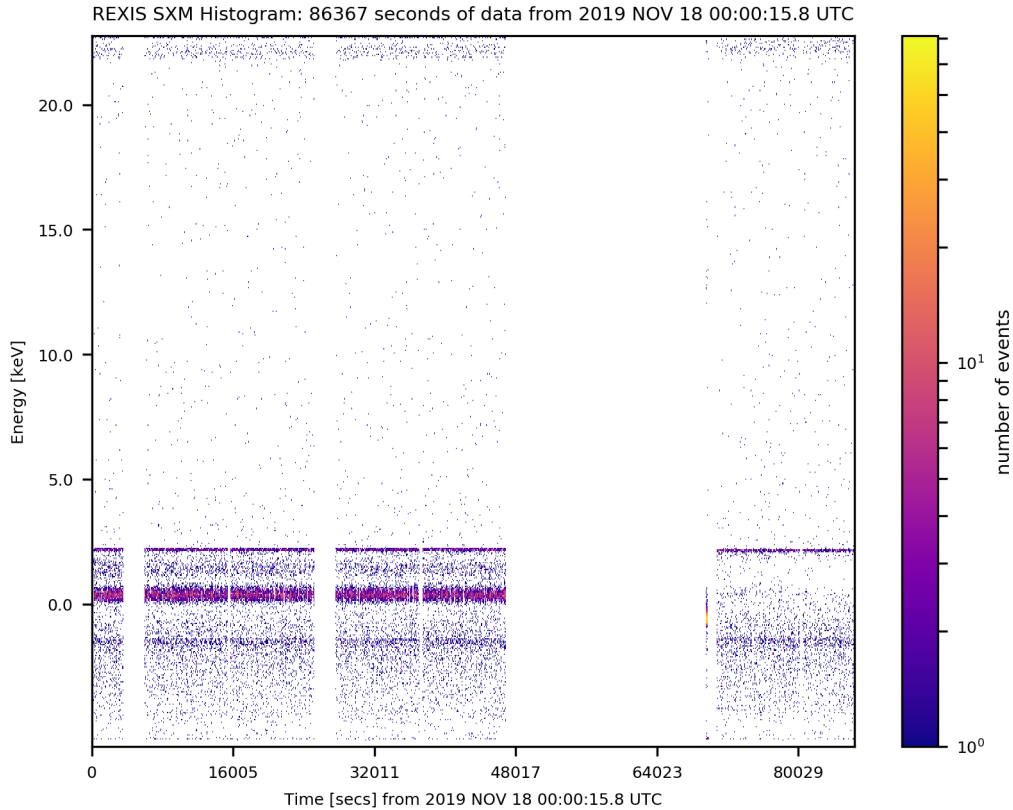


Figure 4-4: SXM count rate histogram on 18 November, 2019. The gap in the histogram is when the instrument was not recording data, and is unrelated to the low count rate anomaly in Orbital R.

#### 4.2.1 ISA #10939

The OSIRIS-REx PI's office opened a formal Incident, Surprise, Anomaly (ISA) investigation into the SXM low count rate. At the conclusion of Orbital B, this investigation was not time sensitive, as REXIS had completed its only observation phase, collected all possible data, and had been powered off according to OSIRIS-REx power mission design.

A fishbone diagram was created to illustrate the possible causes of a low instrument count rate in the SXM. The fishbone diagram included in the SXM low count rate ISA is shown in Figure 4-5.

Each potential cause of the SXM low count rate shown in the fishbone diagram will be explained briefly.

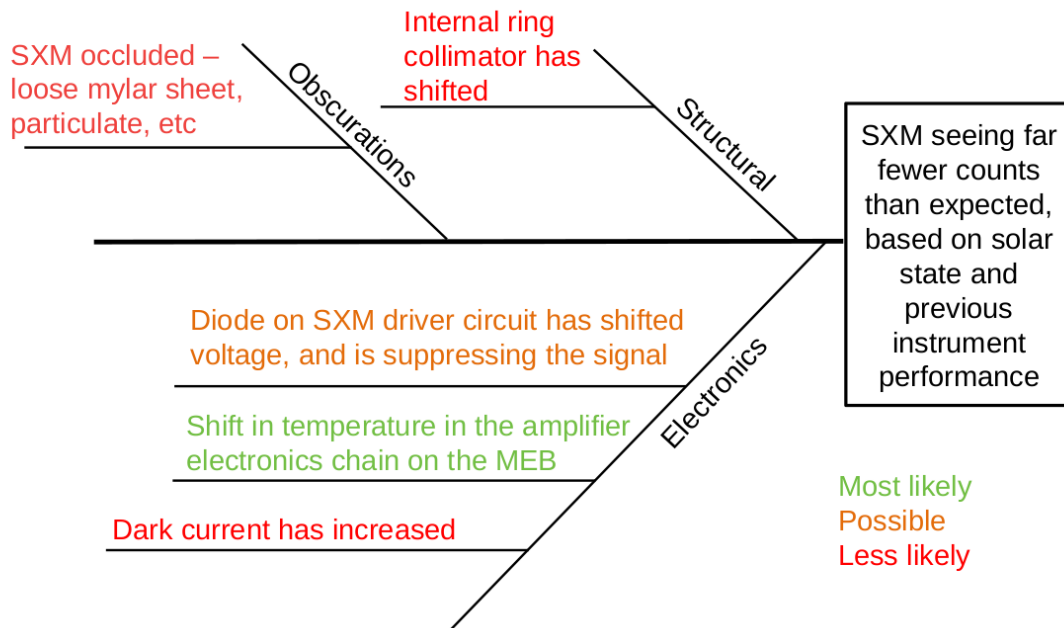


Figure 4-5: Fishbone diagram constructed for OSIRIS-REx ISA #10939

## SXM SDD Detector was Occulted

The SXM SDD detector being occulted was a natural concern for the instrument team. The OSIRIS-REx team discovered that Bennu is an "activated asteroid," which is characterized by dust ejecta from the asteroid's surface [3]. If particulate matter partially or completely occulted the SXM field of view, then the instrument would receive lower counts than predicted. However, it is unlikely that particulate blockage occurred, as the SDD detector is small, and the spacecraft took extreme care to avoid ejecta.

Another way that the SXM might have been physically occulted is if part of the spacecraft, for example foil used to insulate sensitive electronics, became dislodged and migrated to cover the detector. Parts of the spacecraft are lined with mylar, which acts as a thermal insulator. This too is unlikely, as the spacecraft's guidance and control team would notice a change in spacecraft motion.



## Internal Collimator Shifted

The Internal Ring Collimator is attached to the exterior of the preamp housing, and acts as a pinhole for solar x-ray flux. The collimator is attached to the preamp in such a way that if the collimator shifted, it would disconnect critical SXM wiring. This would appear as a total loss of signal in the instrument, rather than as reduced x-ray counts.

It was determined that the SXM did not suffer a complete loss of signal after the SXM observed a solar flare. The timing of the flare detected by the SXM coincided with flare data observed by one of the GOES satellites (Figure 4-6). GOES is an Earth-orbiting satellite constellation that monitors solar phenomena and provides persistent solar observation.

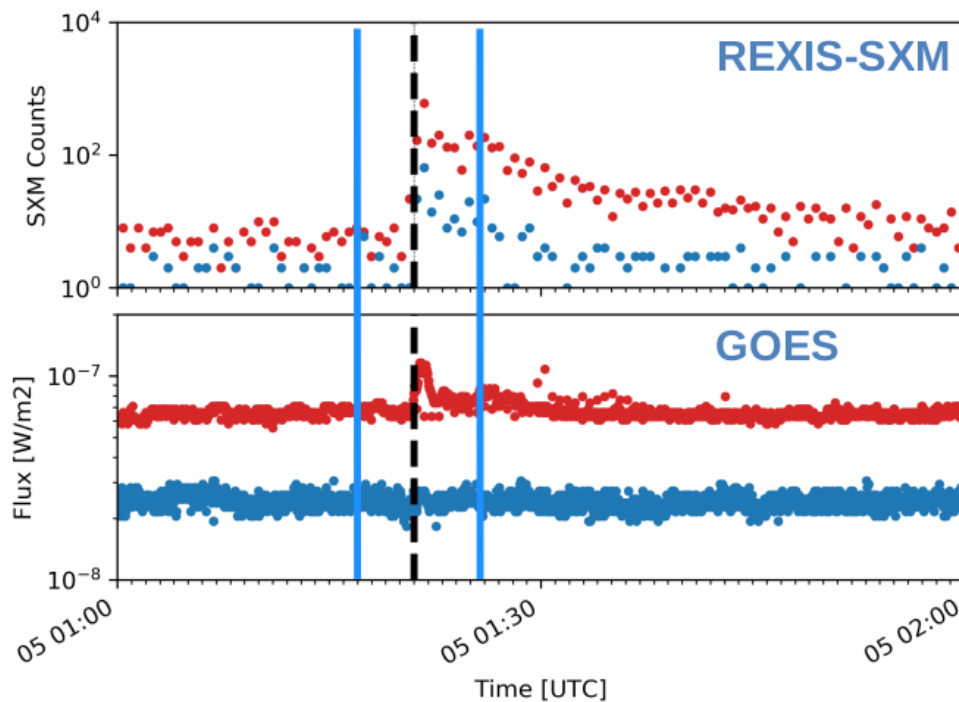


Figure 4-6: Flare Coincidence between the SXM and GOES15.

## Voltage Shift in SXM Driver Circuit

Another possibility considered was that the SXM driver circuit's voltage had shifted. The driver circuit was directly linked to the Analog-to-Digital Converter (ADC) at



Additionally, the second decrease in SXM signal during Orbital R coincided with a thermal change on the spacecraft. Inertial Measurement Unit 1 (IMU1) was switched off, and IMU2 was powered on. The inertial measurement units provide the OSIRIS-REx navigation team with the exact position of the spacecraft, and where it is located with respect to Bennu. When the IMU changeover occurred, the SXM entered a new phase space (shown in Figure X), where the Thermo-Electric Cooler (TEC) temperature decreased, and the temperature doubled in the Detector Electronics (DE), where the REXIS main spectrometer’s video board is housed. The SXM backpack electronics were not effected by this thermal change.

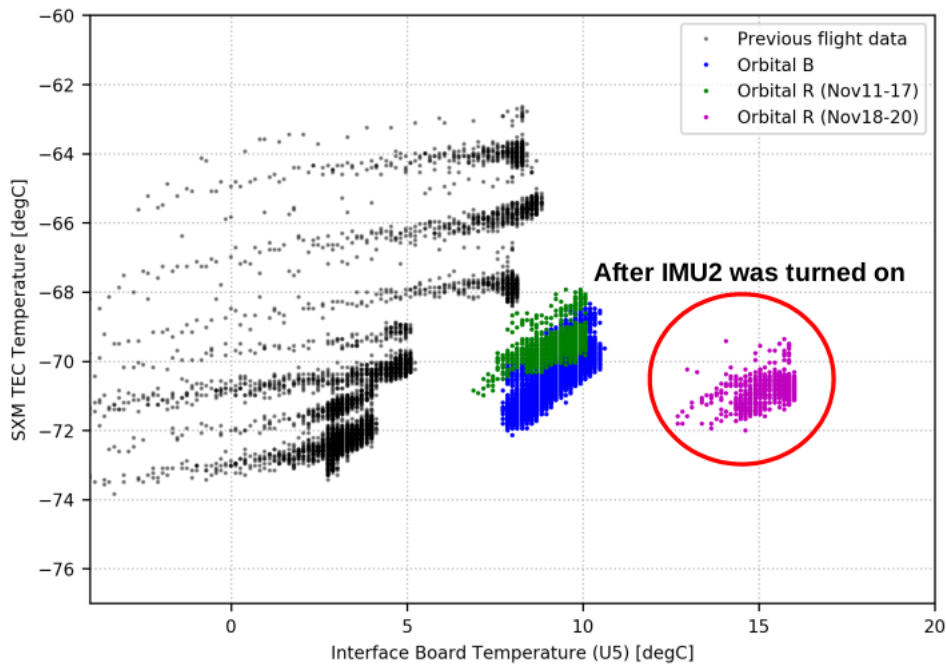


Figure 4-8: SXM Temperature Phase Space.

This dramatic shift in SXM temperature phase space indicated that low count rate was related to a change in MEB temperature. The SXM operated in a new phase space for both Orbital B and Orbital R when compared to previous data, which coincided with lower signal counts. This sensitivity was reported in the ISA #10939 briefing, and it was determined that the SXM was still functional above 3 keV. The low count anomaly presented no threat to any other spacecraft system, and it was recommended that additional work focus on further isolating the root cause.

## 4.2.2 Modeling SXM Instrument Response

Once it had been established that SXM signal was reduced below its expected value, rather than totally lost, efforts were made to recover the signal. If it was possible to recover the signal, SXM data could still be used to measure solar temperature. Solar temperature measurements can be used to calculate solar output, which in turn makes it an essential step in characterizing the Sun's input to Bennu's surface.

The most prominent of these attempts involved rebinning SXM data. Since the SXM was reporting a 100x loss in signal, it was thought that signal could be amplified by rebinning 100 histograms together. The original SXM histograms showed 32 seconds of data. Rebinning histograms combined 3200 seconds of data into a single histogram. Rebinning histogram data required writing additional code to interface with the existing Data Pipeline. Data were separated by collection phase, with Orbital B consisting of one dataset, and Orbital R divided into two, differentiated by which IMU was employed.

Data were rebinned using a sliding bin technique, which used a 3200 second window of data and took averages of the energies of the individual histograms and produced a stacked histogram. Sliding binning was employed to prevent individual high-count histograms from skewing binned data. A limitation to rebinning was that it raised the high energy noise as well as improved signal, which is shown in Figure 4-9. Rebinning also amplified instrument artifact, which binned at an disproportionate rate when compared signal.

Rebinning was ultimately unsuccessful at extracting SXM signal from the low count rate data. Rebinning recovered artifacts back to levels seen in the Internal Calibration, but failed to recover signal to the same levels. Signal could not be recovered to the levels of previous quiet sun data, and further rebinning attempts were abandoned, and efforts were focused on identifying thermally susceptible electronics.

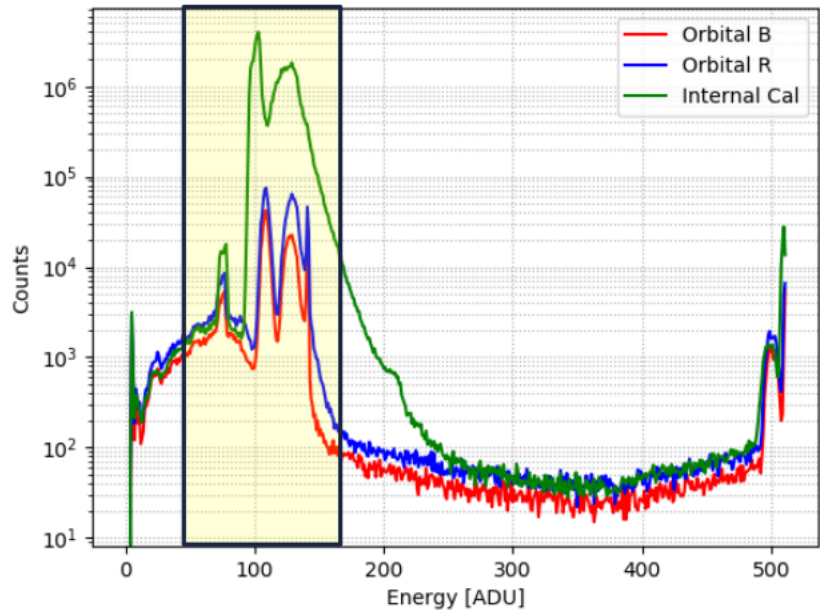


Figure 4-9: SXM Histogram Rebinning. The boxed area surrounds the SXM’s main signal peaks. The peaks at the outer edges of the figure are instrument artifacts.

### 4.3 LTSpice Simulations of Amplification Chain

The SXM amplification chain proved to be the most promising path towards isolating a root cause of the low count anomaly. As was previously explained in Section 4.2.1, the SXM was susceptible to temperature changes in the MEB. This temperature vulnerability was not seen in the ground spare unit, and MIT’s closure due to COVID-19 prevented any further ground testing. Computer simulation of the SXM electronics using LTSpice was chosen as an alternative to physical testing. LTSpice can simulate circuits across multiple temperatures and signal inputs, making it an excellent choice to investigate thermal vulnerability.

LTSpice is a free software distributed by Analog Devices, which allows a user to build and test circuits. LTSpice allows a user to upload proprietary component models, which are produced by electronics hardware companies. These proprietary models incorporate existing LTSpice modeling code and data from a component’s spec sheet.

The opamps used in the SXM amplification chain are produced by MAXIM In-

tegrated, an electrical components company that produces analog and mixed-signal integrated circuits. MAXIM Integrated offers LTSpice models for their components on their website, which are free to download and developed by their engineering staff.

LTSpice has two simulation modes: a netlist, and a schematic. A netlist utilizes Spice syntax and works similar to common coding languages. Components and their values are added to a netlist, and connections to other components are written in LTSpice's netlist syntax. LTSpice schematics are drawn or imported by the user, and have a more robust visual interface. LTSpice schematics are nearly identical to KiCAD and other schematic design software. Both a netlist and schematic can be used to simulate the same circuit.

### **4.3.1 Thermal Variability in Components**

The SXM had an existing netlist from previous simulation, which required minor changes due to software updates. The simulation procedure involved running the circuit for 10ms, with a global electronics temperature range from 0°C to 30°C, run at steps of 5°C. A voltage pulse was used as the input signal, which represented a single detection by the SXM. However, the simulation would not run when given the stepwise temperature procedure. LTSPice refused to run at the upper and lower bounds of the simulation.

The range of testing was modified to run between 20°C and 30°C, within the range of temperatures seen by the MEB during Orbital B and Orbital R. Again, temperatures at the extremes of the range were unable to be simulated by LTSpice. The simulation worked at a temperature of 27°C, but the total time to simulate the circuit increased as the temperature moved closer to 20°C and 30°C.

The increased simulation time was considered to be a result of high-frequency noise, which was believed to indicate that the amplification chain had components that were highly vulnerable to noise, near operational temperatures. This could not be well established with the netlist, as the netlist could not simulate flight temperatures seen in Orbital B, Orbital R, or from any previous flight data with which to compare.

The validity of the existing netlist was called into question, and it was decided

to try to create a schematic of the amplification chain from scratch, to avoid any preexisting errors that could have propagated from the updating of the old netlist.

The amplification chain was recreated in LTSpice using the electronics schematic for the SXM. The MAX4416ESA opamp model was placed in the electronics chain to provide an accurate simulation of signal amplification. The LTSpice schematic of the amplification chain is provided in Figure 4-10.

The simulation was conducted with the same reduced range as the netlist, and again faced the same challenges as the simulation run from the netlist. To eliminate the possibility that the simulations were failing due to computing limitations, the circuit was broken up into five distinct sections, and each contained only one opamp.

Each subcircuit was tested within the same 10°C temperature range. The simulation crashed at same temperatures seen in prior simulations. Consistent simulation failures at the same temperature across multiple configurations was hypothesized to be the result of faulty opamp code. A simulated test circuit was constructed, where the MAX4416ESA opamp was given a generic input and output within its range of operation. The test circuit was run with the same 10°C temperature range, and the range at which the simulation ran properly was constrained to between 22°C and 29°C. This pointed to a limitation in the opamp Spice model, which was confirmed through a series of emails with MAXIM Integrated. The thermal constraint is a known limitation from the manufacturer, which was not published with the Spice model. This was unknown to the REXIS team until April 2020. Additionally, efforts to freeze the opamp model at a local temperature, and run the LTSpice simulation at a different global temperature were unsuccessful.

This revelation made further thermal investigation with LTSpice a fruitless endeavor. The temperatures seen by the MEB during Orbital B and Orbital R were out of range of the model of the opamp used in the amplification chain. While these results are inconclusive, there is further work that can be done towards isolating the root cause of the low count rate anomaly.

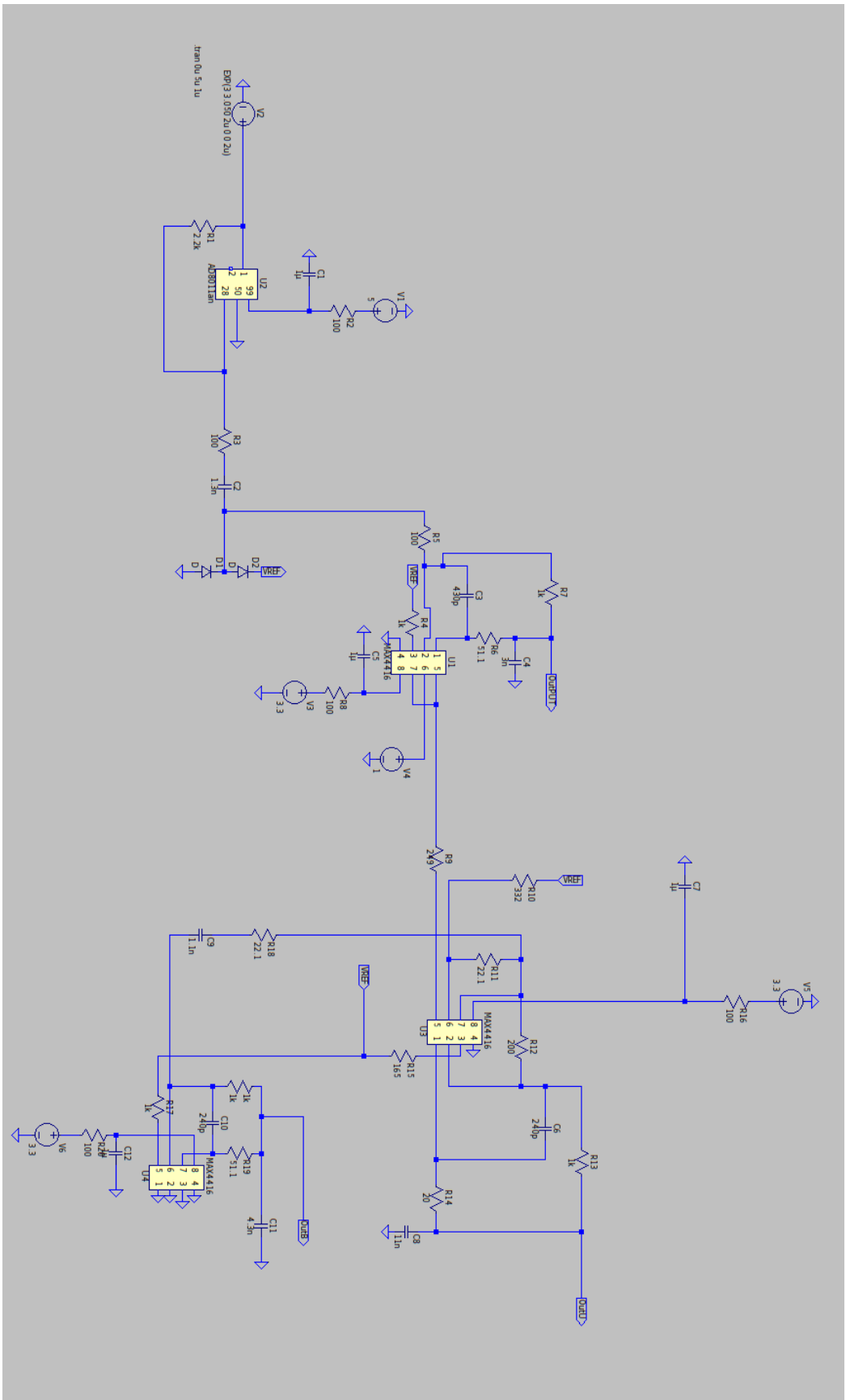


Figure 4-10: The SXM Signal Amplification Chain.



## 4.4 Root Cause Next Steps

The SXM low count rate anomaly remains an open area of investigation. The SXM is a model instrument for other Class D missions, and instrumentation and programmatic lessons learned will allow other instruments to learn and improve from the SXM.

Despite the limitations of circuit simulation, there are avenues to continue the root cause analysis. This section will describe two areas of future work, a continued root cause investigation, and a CAST analysis, which will together serve as the crux of my Master's thesis.

### 4.4.1 Identification of Vulnerable Components

There is still work to be done on a root cause investigation into the low count anomaly. The hypothesis that there are temperature-sensitive components in the SXM amplification chains has not yet been proven wrong. Identifying vulnerable components is important for the NICER team, from which the SXM amplification chain schematic was derived. There is a possibility that NICER is operating with the same vulnerability in their detector chain, and a known vulnerability could be planned for, or worked around by the instrument team.

### 4.4.2 CAST Analysis

Another approach to isolating the cause of the low count rate anomaly is through a Causal Analysis based on System Theory (CAST) investigation. CAST is used to examine the programmatic and control factors that may have influenced an event. While this will not provide further information towards which components in the SXM amplification chain are thermally vulnerable, it offers a way to document lessons learned at a programmatic level. This includes decisions to prioritize some ground tests over others, and decisions made in instrument development. CAST also documents successful control measures that were implemented throughout the project that guarded against other accidents. The goal of this future CAST investigation is to produce a definitive list of lessons that can be used by future instrument teams in their design

and testing process.

# Bibliography

- [1] Amptek. *Manual for the Silicon Drift Diode Detector Element*.
- [2] Bruce Carter and Thomas R. Brown. *Handbook of Operational Amplifiers Applications*. Texas Instruments.
- [3] H. C. Connolly, E. R. Jawin, R. L. Ballouz, K. J. Walsh, T. J. McCoy, D. N. Dellagiustina, K. Burke, E. B. Biehaus, B. Rizk, C. D'Aubigny, V. E. Hamilton, W. F. Bottke, J. P. Dworkin, M. Delbo, S. Tachibana, H. Yurimoto, and Orisis-Rex Team. OSIRIS-REx Sample Science and the Geology of Active Asteroid Bennu. In *82nd Annual Meeting of The Meteoritical Society*, volume 82, page 6209, July 2019.
- [4] Keith Gendreau, Zaven Arzoumanian, and Takashi Okajima. The neutron star interior composition explorer (nicer): An explorer mission of opportunity for soft x-ray timing spectroscopy. *Proceedings of SPIE - The International Society for Optical Engineering*, 8443:13, 09 2012.
- [5] Rajmal Jain, Hemant Dave, AB Shah, N. Vadher, Vishal Shah, G. Ubale, K. Manian, Chirag Solanki, K. Shah, Sumit Kumar, S. Kayasth, V. Patel, Jayshree Trivedi, and M. Deshpande. Solar x-ray spectrometer (soxs) mission on board gsat2 indian spacecraft: The low-energy payload. *Solar Physics*, 227:89–122, 03 2005.
- [6] Michael Jones. The engineering design of the rexis solar x-ray monitor and risk management considerations for resource constrained payload development. Master's thesis, Massachusetts Institute of Technology, 77 Massachusetts Avenue, Cambridge, MA 02219, May 2015.
- [7] Madeline Lambert. A root cause analysis of rexis detection efficiency loss during phase e operations. Master's thesis, Massachusetts Institute of Technology, 77 Massachusetts Avenue, Cambridge, MA 02219, May 2020.
- [8] E. Landi, P. R. Young, K. P. Dere, G. Del Zanna, and H. E. Mason. CHI-ANTI—AN ATOMIC DATABASE FOR EMISSION LINES. XIII. SOFT x-RAY IMPROVEMENTS AND OTHER CHANGES. *The Astrophysical Journal*, 763(2):86, jan 2013.

- [9] D. S. Lauretta, A. E. Bartels, M. A. Barucci, E. B. Bierhaus, R. P. Binzel, W. F. Bottke, H. Campins, S. R. Chesley, B. C. Clark, B. E. Clark, E. A. Cloutis, H. C. Connolly, M. K. Crombie, M. Delbó, J. P. Dworkin, J. P. Emery, D. P. Glavin, V. E. Hamilton, C. W. Hergenrother, C. L. Johnson, L. P. Keller, P. Michel, M. C. Nolan, S. A. Sandford, D. J. Scheeres, A. A. Simon, B. M. Sutter, D. Vokrouhlický, and K. J. Walsh. The osiris-rex target asteroid (101955) bennu: Constraints on its physical, geological, and dynamical nature from astronomical observations. *Meteoritics & Planetary Science*, 50(4):834–849, 2015.
- [10] NASA. *EEE-INST-002: Instructions for EEE Parts Selection, Screening, Qualification, and Derating*.
- [11] NASA. *NPR 8705.4*.
- [12] NASA Goddard Spaceflight Center. *Code 300/Safety and Mission Assurance Directorate. Goddard Procedural Requirement 7120.4: Risk Management*.
- [13] Andrew Poppe, David James, Brian Jacobsmeyer, and Mihály Horányi. First results from the Venetia Burney Student Dust Counter on the New Horizons mission. , 37(11):L11101, June 2010.
- [14] Kevin Stout. Design operations of thermal paths in spacecraft systems. Master’s thesis, Massachusetts Institute of Technology, 77 Massachusetts Avenue, Cambridge, MA 02219, May 2015.
- [15] Janusz Sylwester, S. Kuzin, Yury Kotov, František Fárník, and Fabio Reale. Sphinx: A fast solar photometer in x-rays. *Journal of Astrophysics and Astronomy*, 29:339–343, 06 2008.

# Appendix A

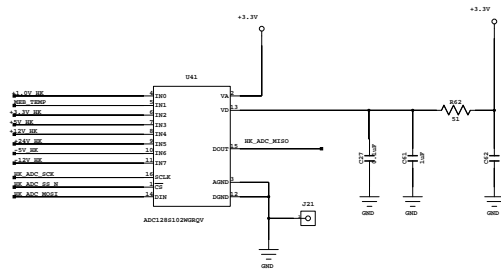
## SXM Circuit Schematics

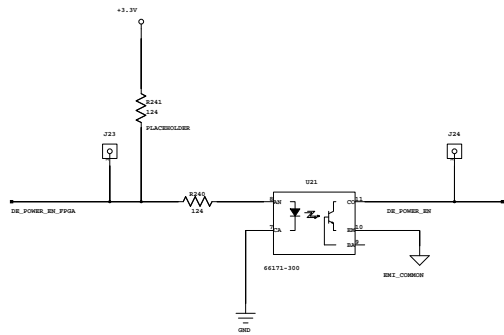
The following Appendix contains the circuit diagrams of all sections of the REXIS SXM. This Appendix also serves as a means through which to document the design of the SXM.

## REXIS MAIN ELECTRONICS BOARD ENGINEERING MODEL SCHEMATICS

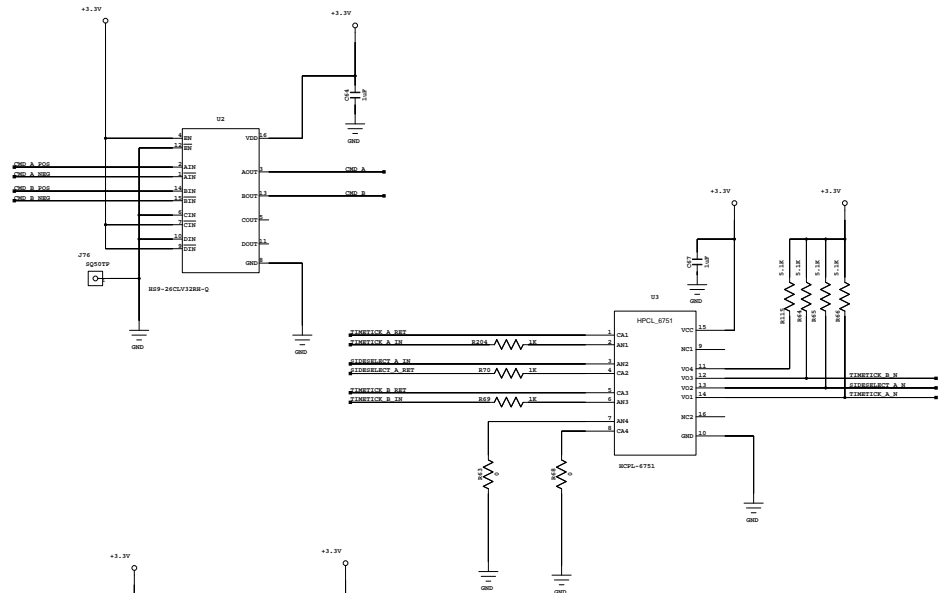
PAGE 1-	TABLE OF CONTENTS
PAGE 2-	TI 8:1 ANALOG TO DIGITAL CONVERTER
PAGE 3-	SPACECRAFT COMM INTERFACE
PAGE 4-	EXTERNAL CONNECTORS - SXM AND PRTS
PAGE 5-	FRANGIBOLT RADIATION COVER RELEASE MECHANISM ACTUATION
PAGE 6-	GROUNDING
PAGE 7-	HOUSEKEEPING VOLTAGE GENERATION
PAGE 8-	AEROFLEX 64MBIT NOR FLASH
PAGE 9-	PRIMARY POWER
PAGE 10-	POWER 1.0V
PAGE 11-	POWER 2.5V
PAGE 12-	POWER 3.3V AND -5V POWER
PAGE 13-	3D-PLUS 1GBIT DDR SDRAM
PAGE 14-	SWITCHES
PAGE 15-	SOLAR X-RAY MONITOR DAC & ADC
PAGE 16-	SOLAR X-RAY MONITOR AMPLITUDE
PAGE 17-	SOLAR X-RAY MONITOR COCKCROFT WALTON HIGH VOLTAGE GENERATOR
PAGE 18-	SOLAR X-RAY MONITOR SHAPING AND AMPLIFICATION
PAGE 19-	SOLAR X-RAY MONITOR TEC DRIVER
PAGE 20-	SOLAR X-RAY MONITOR TEC TEMPERATURE INTERFACE
PAGE 21-	SOLAR X-RAY MONITOR THRESHOLD CONTROL
PAGE 22-	SOLAR X-RAY MONITOR TRIGGER AND TIMING
PAGE 23-	PRT TEMPERATURE MEASUREMENT INTERFACE/PRT INTERFACE
PAGE 24-	VIRTEX-5 BANKS 0-4, CONFIGURATION ADDRESS, OSCILLATOR
PAGE 25-	VIRTEX-5 BANKS 11,12,13 AND 15
PAGE 26-	VIRTEX-5 BANKS 17,18 AND 19 DETECTOR ELECTRONICS CAMERA LINK INTERFACE
PAGE 27-	VIRTEX-5 BANKS 20 AND 21 DDR SDRAM DATA
PAGE 28-	VIRTEX-5 BANKS 23,24,25 AND 26
PAGE 29-	VIRTEX-5 BANKS 5,6,7,8,27, 29
PAGE 30-	VIRTEX-5 MGT I/O AND GND BANKS
PAGE 31-	VIRTEX-5 VCC +1.0V, +2.5V, +3.3V (EXTRA TOC)
PAGE 32-	VIRTEX-5 DECOUPLING

TI 8:1 ANALOG TO DIGITAL CONVERTER

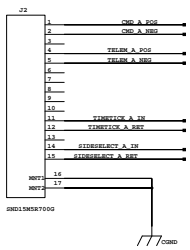




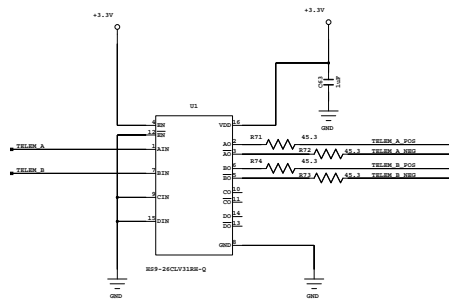
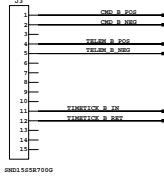
SPACECRAFT COMM INTERFACE  
RS422 TRANSCEIVERS, OPTOCOUPLERS



SIDE A



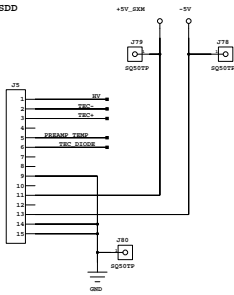
SIDE B



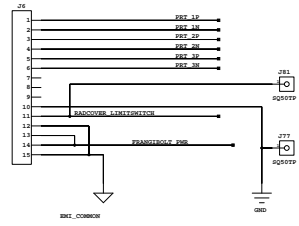


EXTERNAL CONNECTORS - SXM AND PRTS

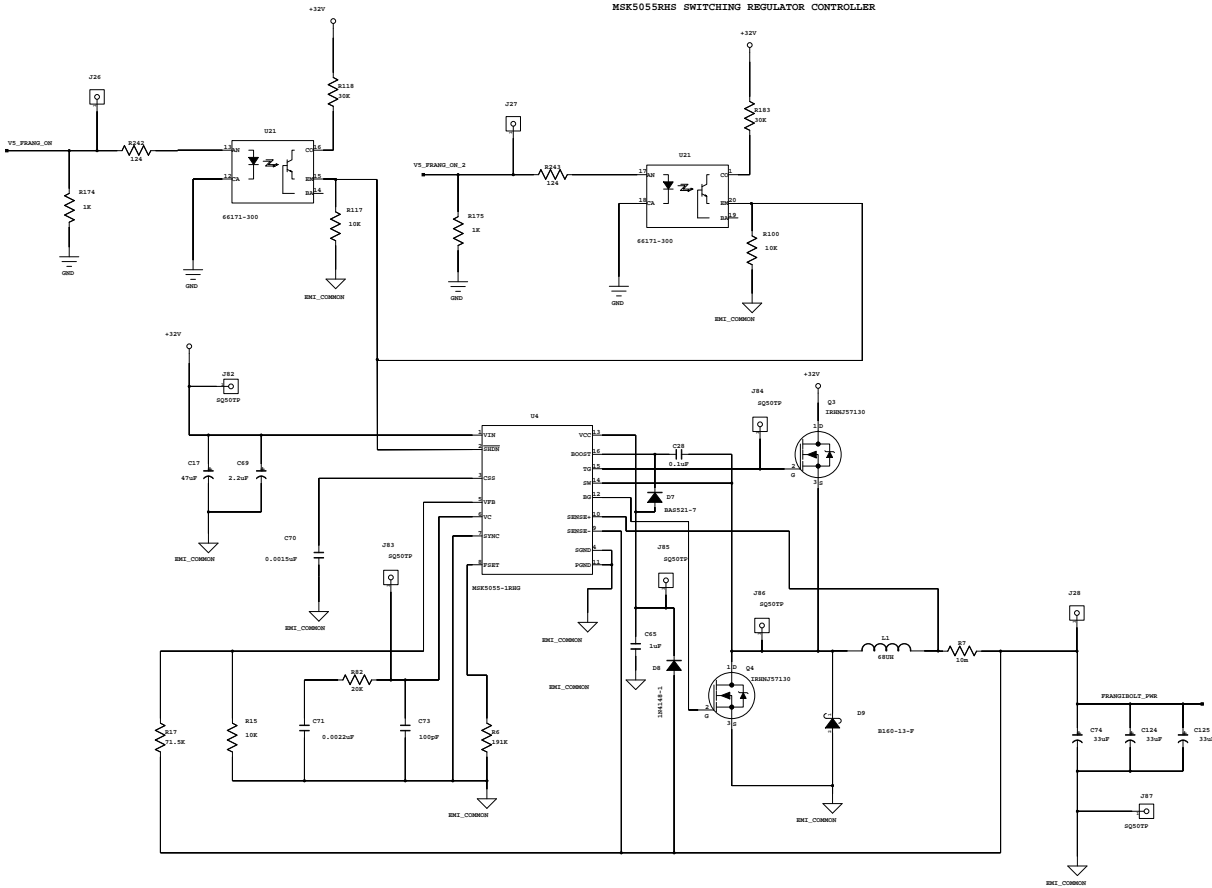
TO PREAMP/SDD

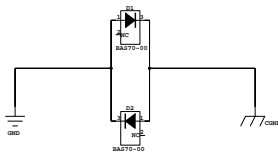


TO PRTS AND LIMIT SWITCH

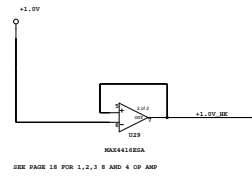
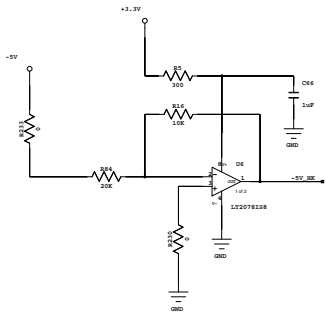
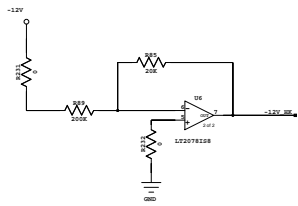
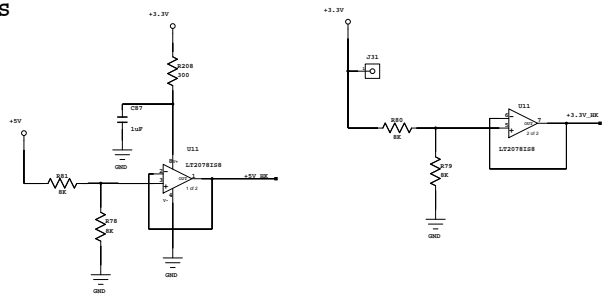
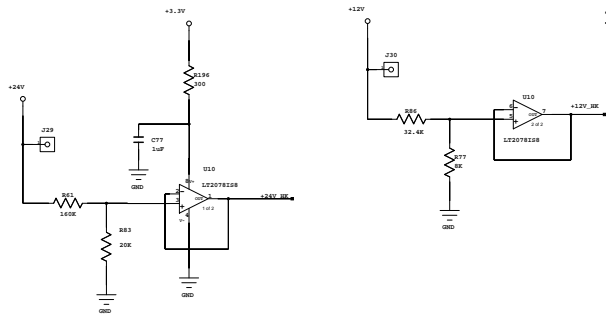


FRANGIBOLT RADIATION COVER RELEASE MECHANISM ACTUATION  
MSK505SRHS SWITCHING REGULATOR CONTROLLER



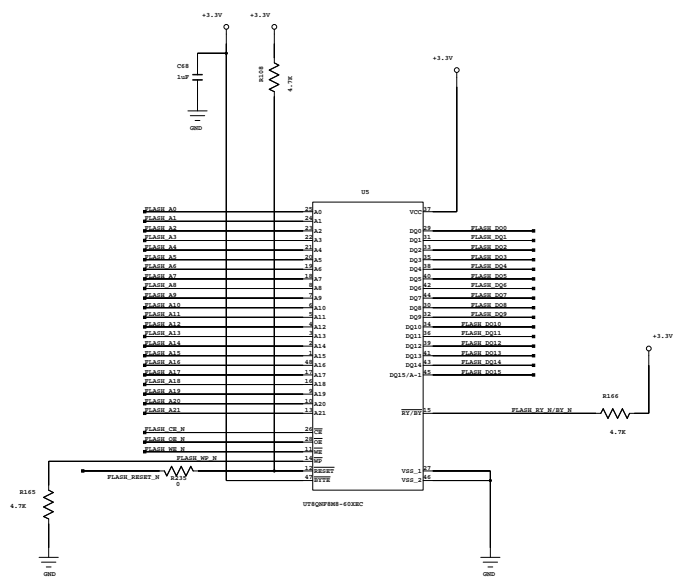


POWERS



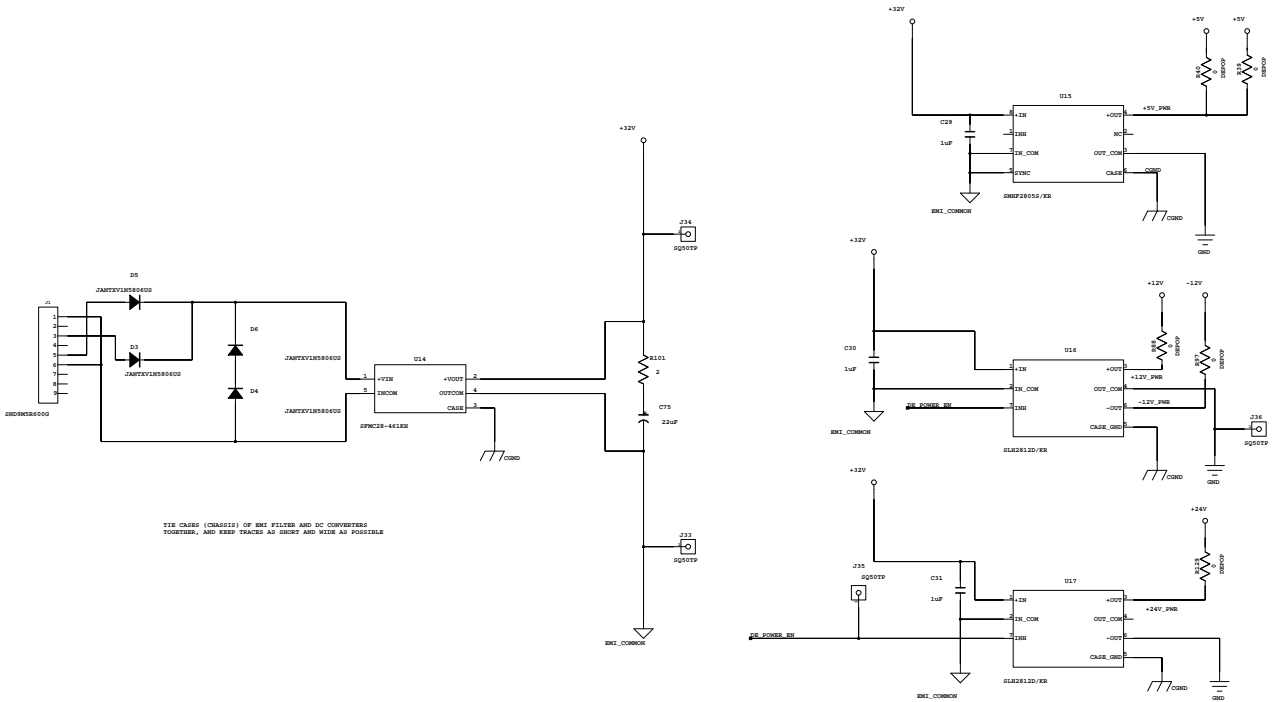
SEE PAGE 16 FOR 1, 2, 3 & AND 4 OP AMP

### AEROFLEX 64MBIT NOR FLASH



PRIMARY POWER

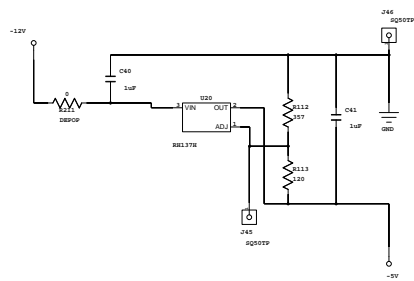
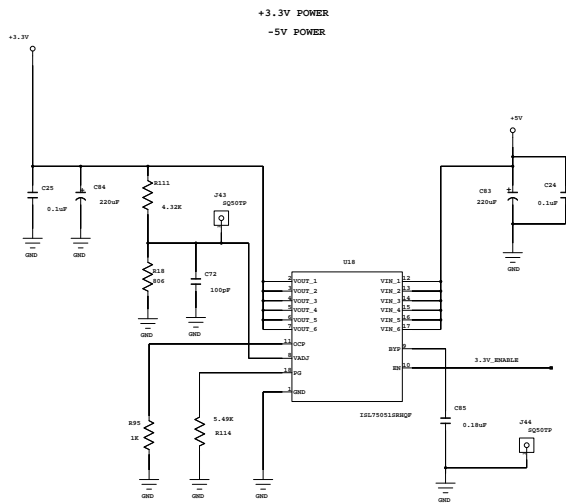
EMI FILTER, +5V, +12V, +24V, -12VDC



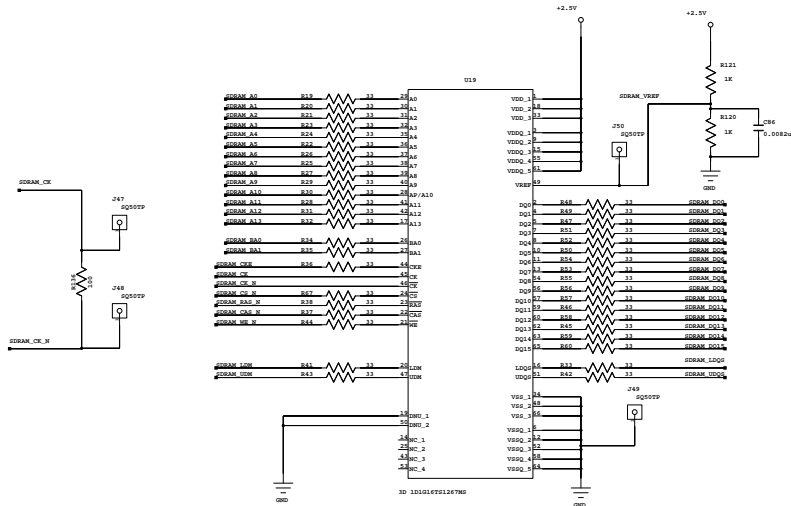




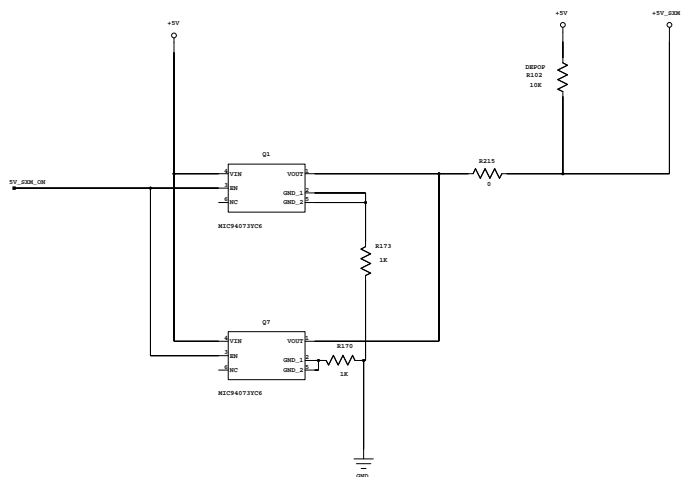




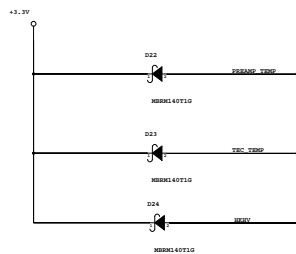
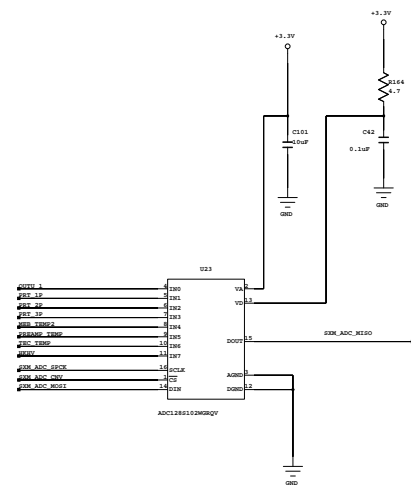
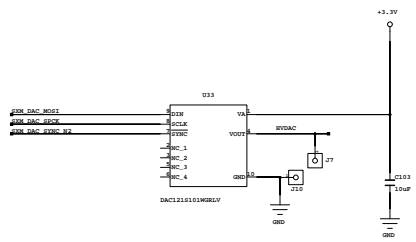
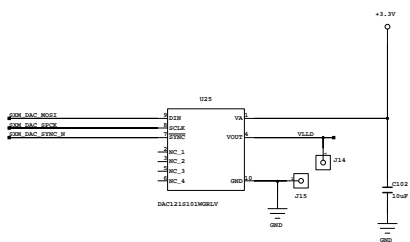
### 3D-PLUS 1GBIT DDR SDRAM



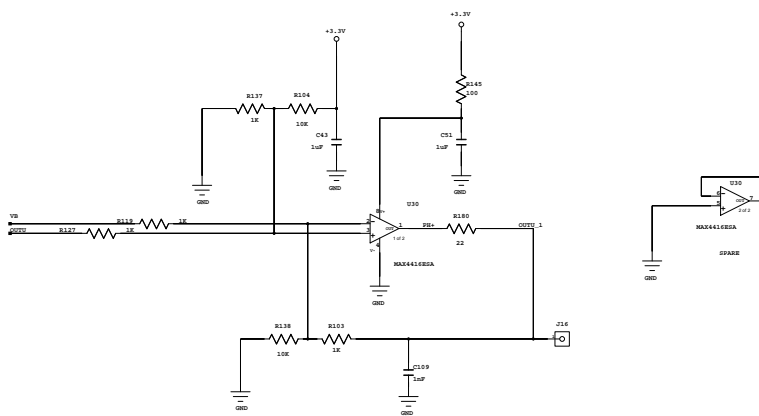
MOSFET SWITCH  
DETECTOR ELECTRONICS 5V RAIL  
SOLAR X-RAY MONITOR 5V RAIL



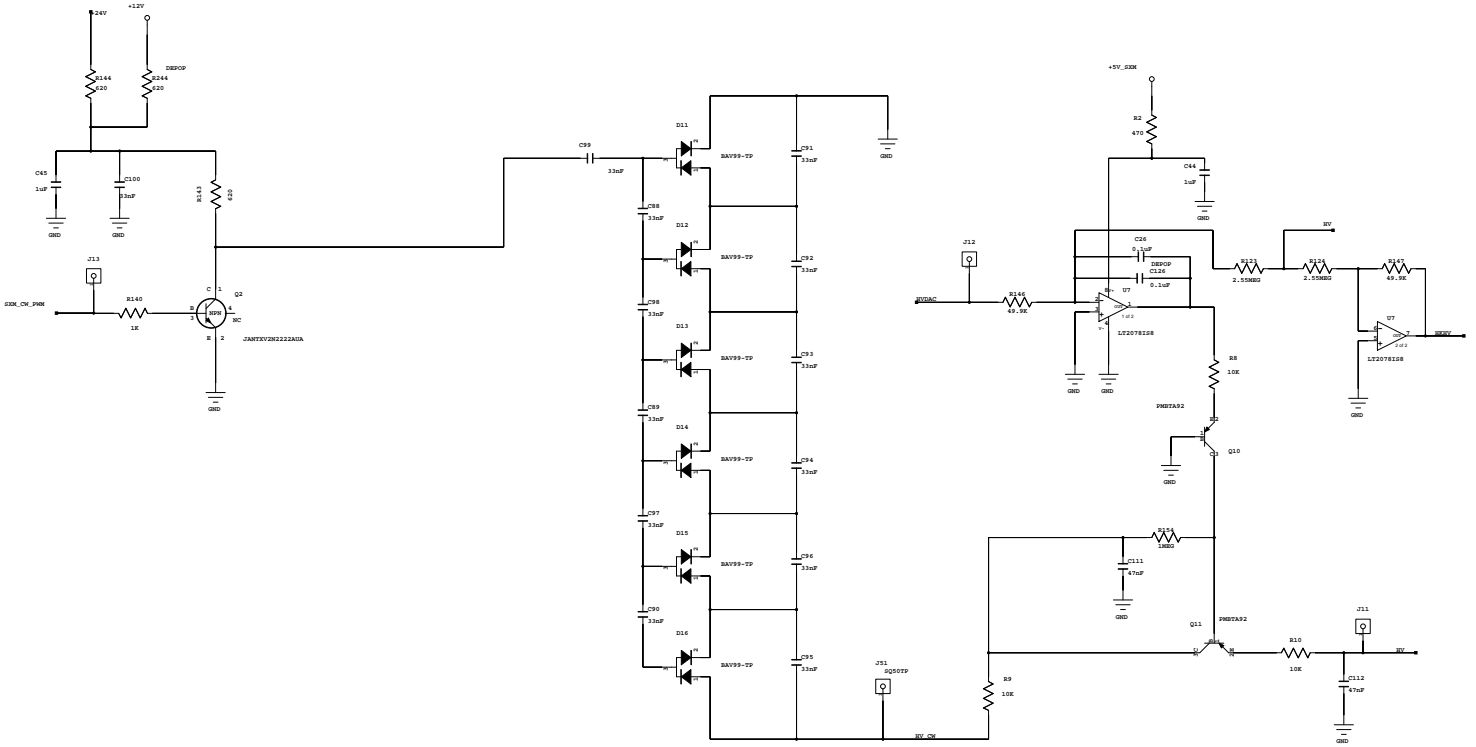
SOLAR X-RAY MONITOR DAC & ADC



SOLAR X-RAY MONITOR AMPLITUDE CAPTURE

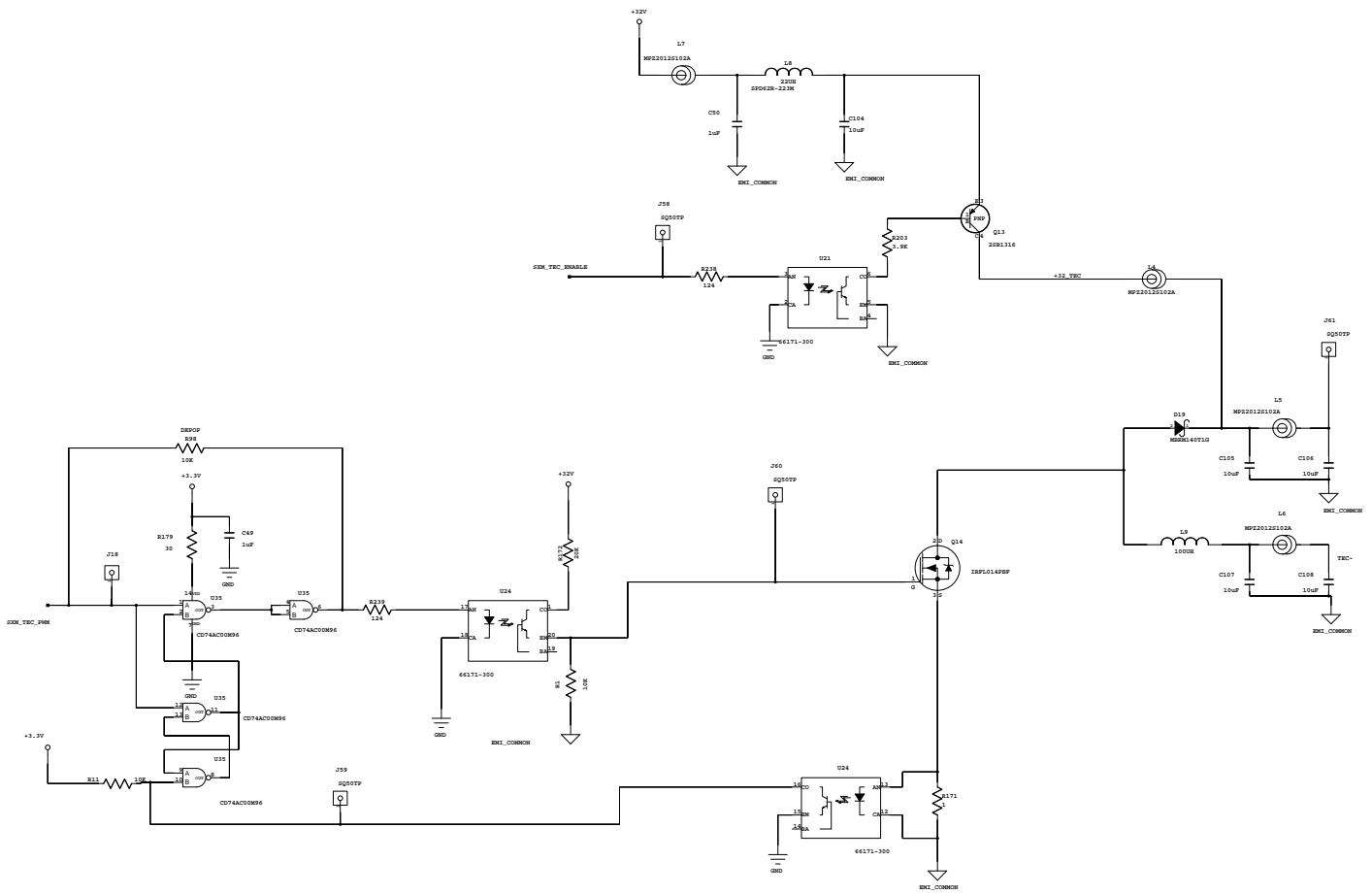


SOLAR X-RAY MONITOR COCKCROFT WALTON HIGH VOLTAGE GENERATOR



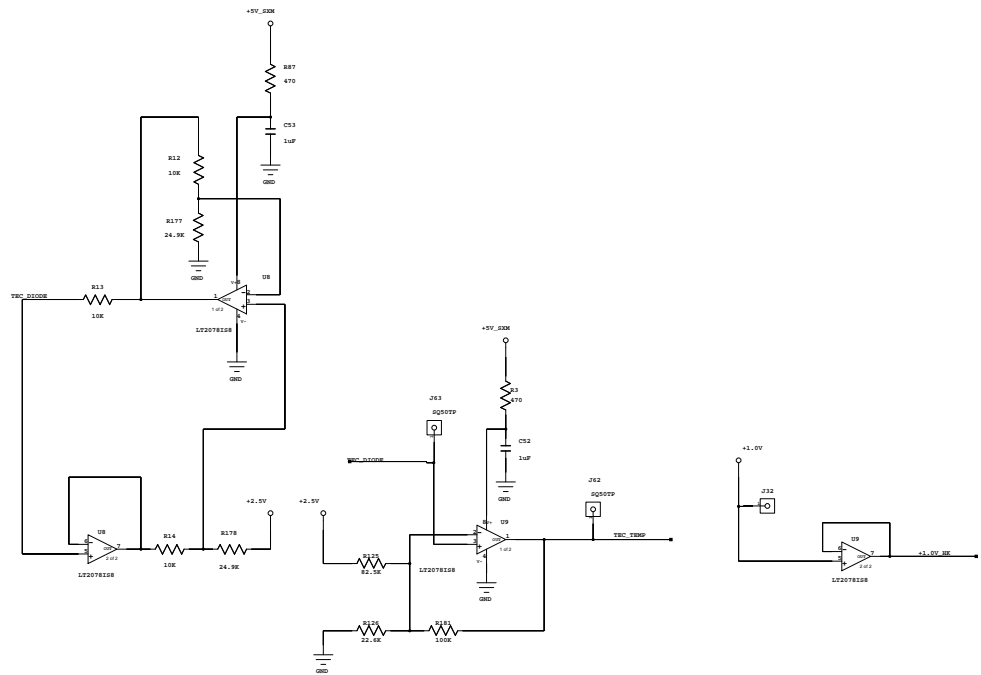


SOLAR X-RAY MONITOR TEC DRIVER

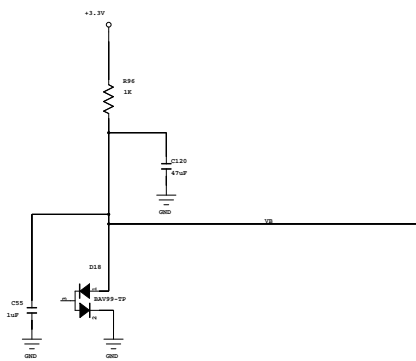




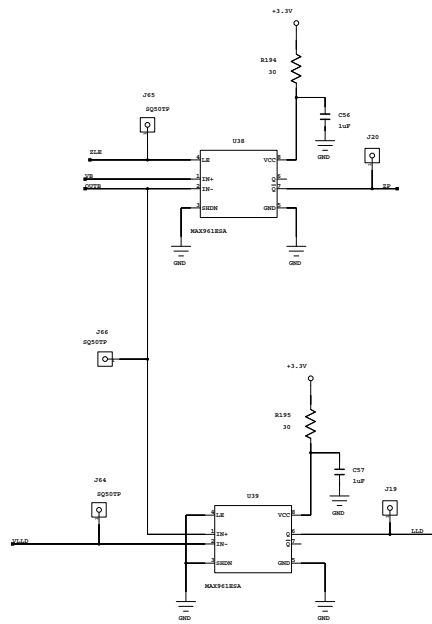
SOLAR X-RAY MONITOR TEC TEMPERATURE INTERFACE



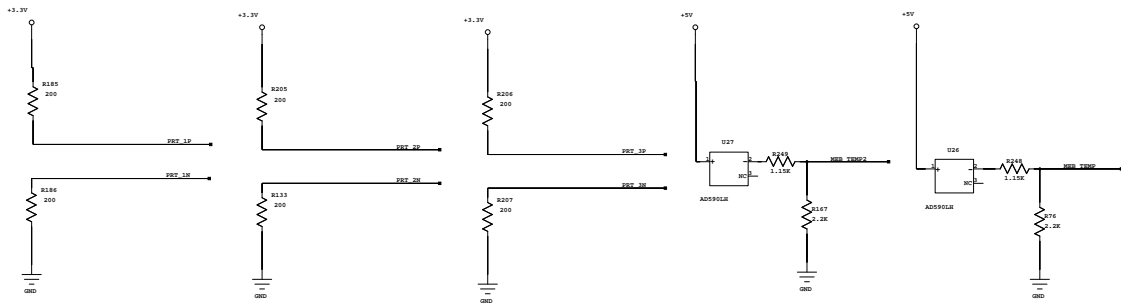
SOLAR X-RAY MONITOR THRESHOLD CONTROL



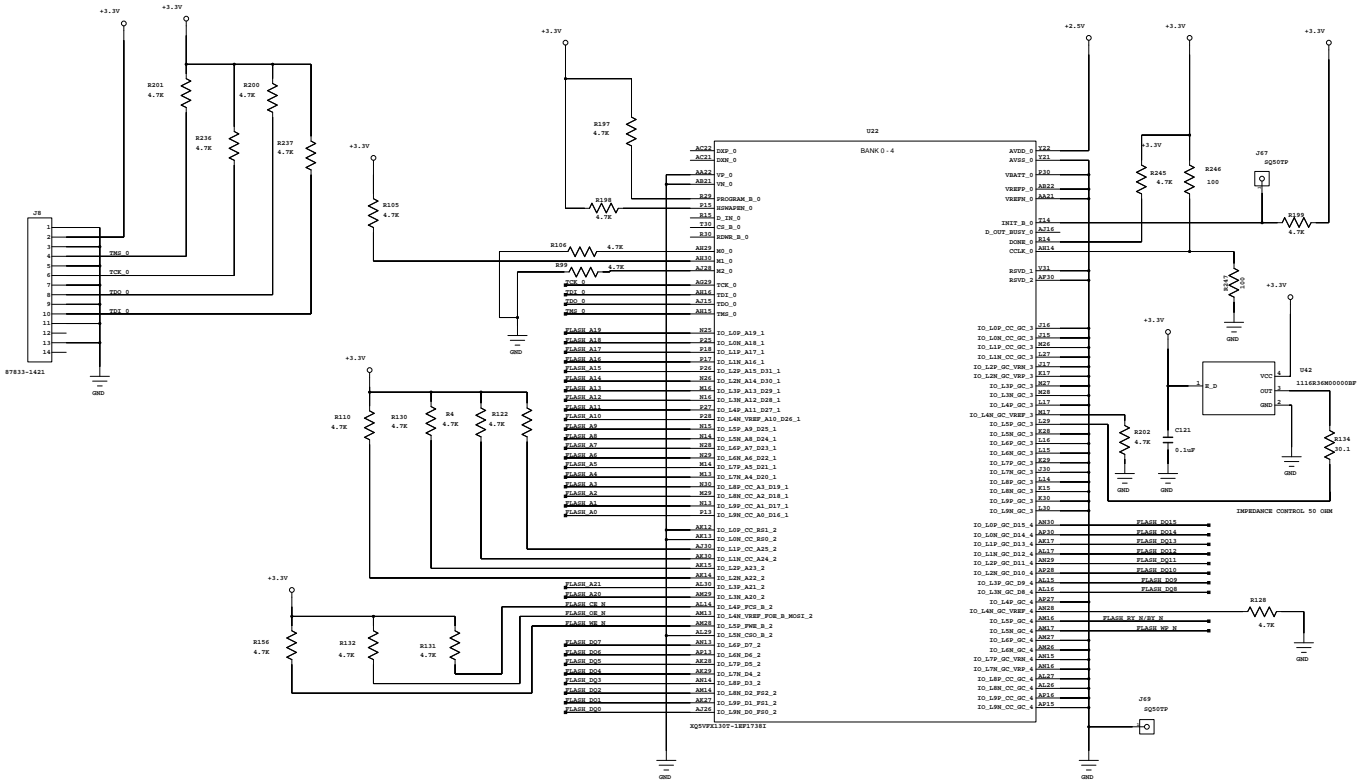
### SOLAR X-RAY MONITOR TRIGGER AND TIMING



PRT TEMPERATURE MEASUREMENT INTERFACE



VIRTEX-5 BANKS 0-4  
CONFIGURATION ADDRESS  
OSCILLATOR

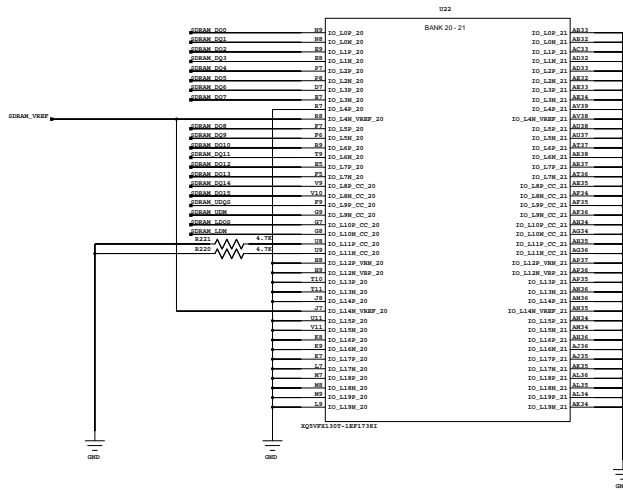






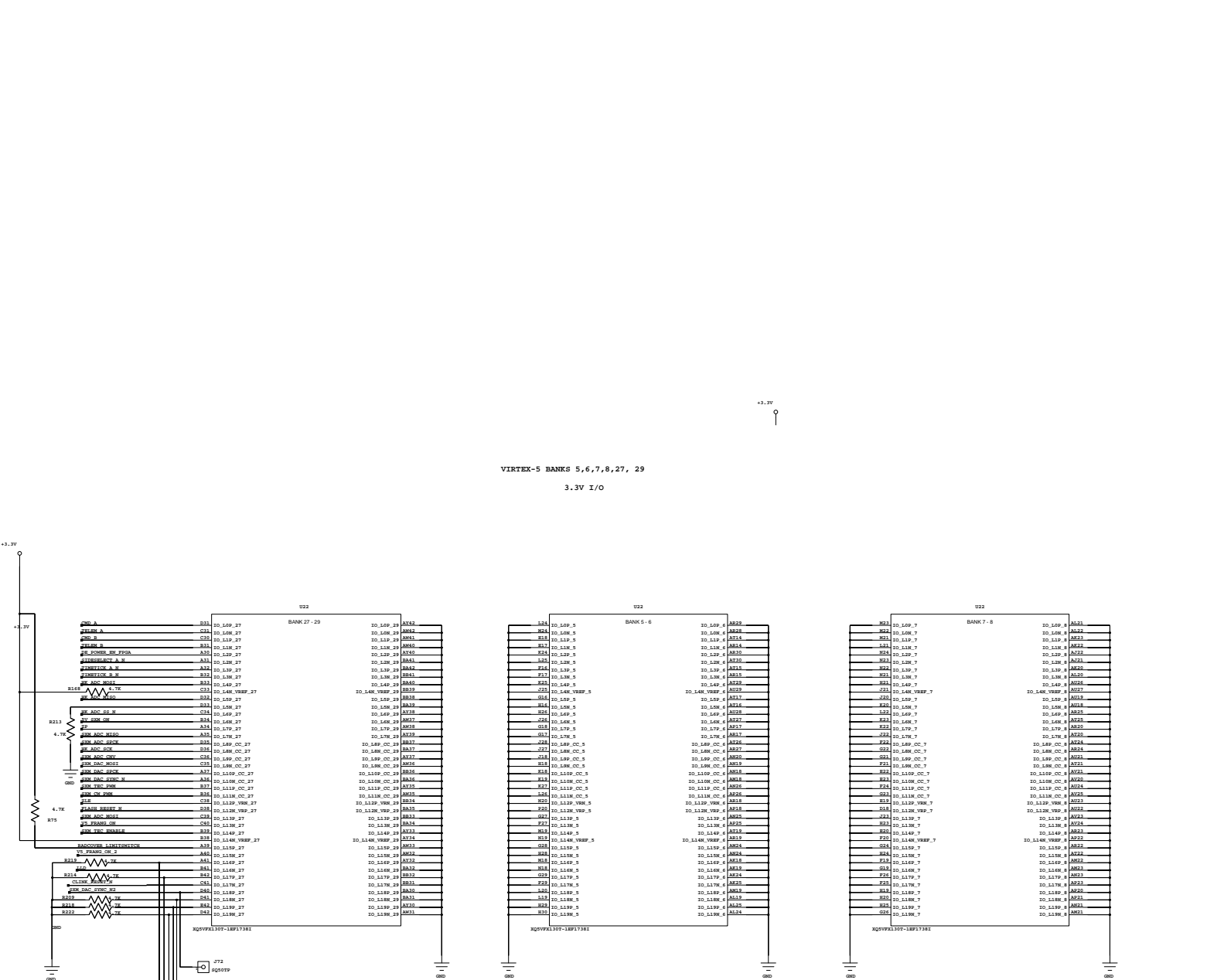
VIRTEX-5 BANKS 20 AND 21

DDR SDRAM DATA









VIRTEX-5 BANKS 5,6,7,8,27, 29  
3.3V I/O

VIRTEX-5 MGT I/O AND GND BANKS

022

F24	GND174	GND241	J22
F24	GND175	GND242	J22
F24	GND176	GND243	J22
F24	GND177	GND244	J22
F24	GND178	GND245	J22
F24	GND179	GND246	J22
F24	GND180	GND247	J22
F24	GND181	GND248	J22
F24	GND182	GND249	J22
F24	GND183	GND250	J22
F24	GND184	GND251	J22
F24	GND185	GND252	J22
F24	GND186	GND253	J22
F24	GND187	GND254	J22
F24	GND188	GND255	J22
F24	GND189	GND256	J22
F24	GND190	GND257	J22
F24	GND191	GND258	J22
F24	GND192	GND259	J22
F24	GND193	GND260	J22
F24	GND194	GND261	J22
F24	GND195	GND262	J22
F24	GND196	GND263	J22
F24	GND197	GND264	J22
F24	GND198	GND265	J22
F24	GND199	GND266	J22
F24	GND200	GND267	J22
F24	GND201	GND268	J22
F24	GND202	GND269	J22
F24	GND203	GND270	J22
F24	GND204	GND271	J22
F24	GND205	GND272	J22
F24	GND206	GND273	J22
F24	GND207	GND274	J22
F24	GND208	GND275	J22
F24	GND209	GND276	J22
F24	GND210	GND277	J22
F24	GND211	GND278	J22
F24	GND212	GND279	J22
F24	GND213	GND280	J22
F24	GND214	GND281	J22
F24	GND215	GND282	J22
F24	GND216	GND283	J22
F24	GND217	GND284	J22
F24	GND218	GND285	J22
F24	GND219	GND286	J22
F24	GND220	GND287	J22
F24	GND221	GND288	J22
F24	GND222	GND289	J22
F24	GND223	GND290	J22
F24	GND224	GND291	J22
F24	GND225	GND292	J22
F24	GND226	GND293	J22
F24	GND227	GND294	J22
F24	GND228	GND295	J22
F24	GND229	GND296	J22
F24	GND230	GND297	J22
F24	GND231	GND298	J22
F24	GND232	GND299	J22
F24	GND233	GND300	J22
F24	GND234	GND301	J22
F24	GND235	GND302	J22
F24	GND236	GND303	J22
F24	GND237	GND304	J22
F24	GND238	GND305	J22
F24	GND239	GND306	J22
F24	GND240	GND307	J22
F24	GND241	GND308	J22
F24	GND242	GND309	J22
F24	GND243	GND310	J22
F24	GND244	GND311	J22
F24	GND245	GND312	J22
F24	GND246	GND313	J22
F24	GND247	GND314	J22
F24	GND248	GND315	J22
F24	GND249	GND316	J22
F24	GND250	GND317	J22
F24	GND251	GND318	J22
F24	GND252	GND319	J22
F24	GND253	GND320	J22
F24	GND254	GND321	J22
F24	GND255	GND322	J22
F24	GND256	GND323	J22
F24	GND257	GND324	J22
F24	GND258	GND325	J22
F24	GND259	GND326	J22
F24	GND260	GND327	J22

XQVVPX1377-18P17381

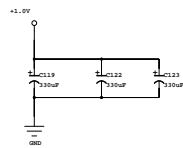
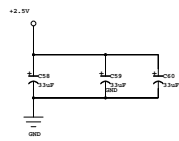
022

F2	GND1	GND1	J23
F2	GND2	GND2	J23
F2	GND3	GND3	J23
F2	GND4	GND4	J23
F2	GND5	GND5	J23
F2	GND6	GND6	J23
F2	GND7	GND7	J23
F2	GND8	GND8	J23
F2	GND9	GND9	J23
F2	GND10	GND10	J23
F2	GND11	GND11	J23
F2	GND12	GND12	J23
F2	GND13	GND13	J23
F2	GND14	GND14	J23
F2	GND15	GND15	J23
F2	GND16	GND16	J23
F2	GND17	GND17	J23
F2	GND18	GND18	J23
F2	GND19	GND19	J23
F2	GND20	GND20	J23
F2	GND21	GND21	J23
F2	GND22	GND22	J23
F2	GND23	GND23	J23
F2	GND24	GND24	J23
F2	GND25	GND25	J23
F2	GND26	GND26	J23
F2	GND27	GND27	J23
F2	GND28	GND28	J23
F2	GND29	GND29	J23
F2	GND30	GND30	J23
F2	GND31	GND31	J23
F2	GND32	GND32	J23
F2	GND33	GND33	J23
F2	GND34	GND34	J23
F2	GND35	GND35	J23
F2	GND36	GND36	J23
F2	GND37	GND37	J23
F2	GND38	GND38	J23
F2	GND39	GND39	J23
F2	GND40	GND40	J23
F2	GND41	GND41	J23
F2	GND42	GND42	J23
F2	GND43	GND43	J23
F2	GND44	GND44	J23
F2	GND45	GND45	J23
F2	GND46	GND46	J23
F2	GND47	GND47	J23
F2	GND48	GND48	J23
F2	GND49	GND49	J23
F2	GND50	GND50	J23
F2	GND51	GND51	J23
F2	GND52	GND52	J23
F2	GND53	GND53	J23
F2	GND54	GND54	J23
F2	GND55	GND55	J23
F2	GND56	GND56	J23
F2	GND57	GND57	J23
F2	GND58	GND58	J23
F2	GND59	GND59	J23
F2	GND60	GND60	J23
F2	GND61	GND61	J23
F2	GND62	GND62	J23
F2	GND63	GND63	J23
F2	GND64	GND64	J23
F2	GND65	GND65	J23
F2	GND66	GND66	J23
F2	GND67	GND67	J23
F2	GND68	GND68	J23
F2	GND69	GND69	J23
F2	GND70	GND70	J23
F2	GND71	GND71	J23
F2	GND72	GND72	J23
F2	GND73	GND73	J23
F2	GND74	GND74	J23
F2	GND75	GND75	J23
F2	GND76	GND76	J23
F2	GND77	GND77	J23
F2	GND78	GND78	J23
F2	GND79	GND79	J23
F2	GND80	GND80	J23
F2	GND81	GND81	J23
F2	GND82	GND82	J23
F2	GND83	GND83	J23
F2	GND84	GND84	J23
F2	GND85	GND85	J23
F2	GND86	GND86	J23

XQVVPX1377-18P17381



VIRTEX-5 DECOUPLING





# Appendix B

## Simulation Code

The following Appendix contains python code developed for SXM data analysis.

### B.1 SXM Simulated Instrument Response Code

The following section contains SXM simulated response code used to attempt to fit SXM flight data to Chianti solar abundance models. This code implements SXM Data Pipeline code written by the REXIS Science Team.

```
#!/usr/bin/env python3
# -*- coding: utf-8 -*-
"""
Created on Fri Jun 28 09:26:40 2019

@author: andrewcummings
"""

import ChiantiPy.core as ch
import ChiantiPy.tools.filters as cf
import matplotlib.pyplot as plt
import numpy as np
```

```

#temp1 = np.arange(1.e+6,625e+4,25.e+4)
#temp2 = np.arange(65.e+5,10.e+6,5.e+5)
#temp3 = np.arange(10.e+6,21.e+6,1.e+6)
#temp12 = np.concatenate((temp1,temp2),axis=None)
#T = np.concatenate((temp12,temp3),axis=None)

""" file name """
def chianti_spectra_generation(file,abundance):
    file ='sun_photospheric_1998_grevesse_highres.npz'
    #abundances:
        # sun_photospheric_1998_grevesse ,
        sun_photospheric_2015_scott_ext ,
        sun_coronal_feldman_1992_ext ,
        sun_coronal_2012_schmelz_ext

    E= np.arange(0.0495, 25.0005, 0.005)
    T = np.array([ 0.5, 0.6, 0.7, 0.8, 0.9, 1. ,
1.1, 1.2, 1.3,
1.4, 1.5, 1.6, 1.7, 1.8,
1.9, 2. , 2.1, 2.2,
2.3, 2.4, 2.5, 2.6, 2.7,
2.8, 2.9, 3. , 3.1,
3.2, 3.3, 3.4, 3.5, 3.6,
3.7, 3.8, 3.9, 4. ,
4.1, 4.2, 4.3, 4.4, 4.5,
4.6, 4.7, 4.8, 4.9,
5. , 5.1, 5.2, 5.3, 5.4,

```



5.5, 5.6, 5.7, 5.8,  
5.9, 6. , 6.1, 6.2, 6.3,  
6.4, 6.5, 6.6, 6.7,  
6.8, 6.9, 7. , 7.1, 7.2,  
7.3, 7.4, 7.5, 7.6,  
7.7, 7.8, 7.9, 8. , 8.1,  
8.2, 8.3, 8.4, 8.5,  
8.6, 8.7, 8.8, 8.9, 9. ,  
9.1, 9.2, 9.3, 9.4,  
9.5, 9.6, 9.7, 9.8, 9.9,  
10. , 10.1, 10.2, 10.3,  
10.4, 10.5, 10.6, 10.7, 10.8,  
10.9, 11. , 11.1, 11.2,  
11.3, 11.4, 11.5, 11.6, 11.7,  
11.8, 11.9, 12. , 12.1,  
12.2, 12.3, 12.4, 12.5, 12.6,  
12.7, 12.8, 12.9, 13. ,  
13.1, 13.2, 13.3, 13.4, 13.5,  
13.6, 13.7, 13.8, 13.9,  
14. , 14.1, 14.2, 14.3, 14.4,  
14.5, 14.6, 14.7, 14.8,  
14.9, 15. , 15.1, 15.2, 15.3,  
15.4, 15.5, 15.6, 15.7,  
15.8, 15.9, 16. , 16.1, 16.2,  
16.3, 16.4, 16.5, 16.6,  
16.7, 16.8, 16.9, 17. , 17.1,  
17.2, 17.3, 17.4, 17.5,  
17.6, 17.7, 17.8, 17.9, 18. ,  
18.1, 18.2, 18.3, 18.4,  
18.5, 18.6, 18.7, 18.8, 18.9,

```

19. , 19.1, 19.2, 19.3,
19.4, 19.5, 19.6, 19.7, 19.8,
19.9, 20. ])

```

```

T=T*1.e6

```

```

#T= np.logspace(5, 7, 50)
s= ch.spectrum(T, wavelength= 12.4/E, eDensity= 1e9,
em= 1e27, filter= (cf.gaussianR, 10000),
abundance='sun_photospheric_1998_grevesse',
minAbund= 1e-6,verbose=1)

```

```

I= s.Spectrum

```

```

#plt.plot(E, I['intensity'][:,1])
#plt.xlabel('Energy [keV]')
#plt.ylabel(I['ylabel'][:, -2])
np.savez_compressed(file, I,E=E,T=T,
wavelength = 12.4/E)
f = np.load(file)
s= dict(f['arr_0'].tolist())
wvl = s['wavelength']
T=f['T']
T=T/1.e6
E = 12.4/wvl
intensity= s['intensity']
for i in range(len(T)):

```

```

        intensity[i,:] = intensity[i,:]*4.06*1.e6*(wvl)**3
data = intensity
np.savez_compressed(file , E=E,
data=data.T,T=T)

```

## B.2 SXM Histogram Rebinning

Code used to rebin Orbital B and Orbital R flight data to attempt to recover x-ray signal. SXM flight data was loaded manually into the rebinner because of x-ray count rate differences that existed between the two sections of Orbital R. Level 0 SXM flight data is delineated by "YYYYDDD," where DDD is the day of the year that data was recorded.

```

import h5py as h
import math as m
import numpy as np

'2019182_L0.h5', '2019183_L0.h5', '2019184_L0.h5',
'2019185_L0.h5', '2019186_L0.h5',
        '2019187_L0.h5', '2019188_L0.h5', '2019189_L0.h5',
'2019190_L0.h5', '2019191_L0.h5',
        '2019192_L0.h5', '2019193_L0.h5', '2019194_L0.h5',
'2019195_L0.h5', '2019196_L0.h5']
file=[ '2019197_L0.h5', '2019198_L0.h5', '2019199_L0.h5',
'2019200_L0.h5', '2019201_L0.h5',
        '2019202_L0.h5', '2019203_L0.h5',
        '2019204_L0.h5', '2019205_L0.h5', '2019206_L0.h5',
        '2019207_L0.h5', '2019208_L0.h5',

```

```

'2019209_L0.h5', '2019210_L0.h5', '2019211_L0.h5',
'2019212_L0.h5', '2019213_L0.h5',
'2019214_L0.h5', '2019215_L0.h5', '2019216_L0.h5',
'2019217_L0.h5', '2019218_L0.h5']

```

```

#dtype([( 'sxm_period', '<u2'), ('TotalEventsCnt', '<u2'),
('underflowEventCnt', '<u2'), ('overflowEventCnt', '<u2'),
('bin', '<u2', (512,)), ('scTime(subsecs)', '<f8'),
('scTime(secs)', '<f8'), ('scGlobalCount', '<f8')])

```

```

#dtype([( 'Sync', 'S30'), ('Length', '<u4'),
('PacketID', '<u4'), ('GlobalCount', '<u4'),
('Time(secs)', '<u4'), ('Time(subsecs)', '<u4'),
('LocalCount', '<u4'), ('LocalTotal', '<u4'),
('SpacecraftTime', '<u4')])

```

```

def concatenate_hdr(ENTRY):

```

```

    f000 = h.File(file[0], 'r')
    b000 = f000['data/tlm_sxm_data/hdr'][ENTRY]
    for i in range(1,18):
        # NEED TO CHANGE THIS TO range(1,len(file)) [this currently
        # throws an error for 18th or 19th entry in file]
        f_now = h.File(file[i], 'r')
        b_now = f_now['data/tlm_sxm_data/hdr'][ENTRY]
        if i == 1:
            c_now = np.concatenate((b000,b_now),0)
            current = c_now
        else:
            c_now = np.concatenate((current,b_now),0)
            current = c_now

    return current

```

```

def concatenate_prehdr(ENTRY):
    f000 = h.File(file[0], 'r')
    b000 = f000['data/tlm_sxm_data/pre_hdr'][ENTRY]
    for i in range(1,18):
        # NEED TO CHANGE THIS TO range(1,len(file)) [this currently
        # throws an error for 18th or 19th entry in file]
        f_now = h.File(file[i], 'r')
        b_now = f_now['data/tlm_sxm_data/pre_hdr'][ENTRY]
        if i == 1:
            c_now = np.concatenate((b000,b_now),0)
            current = c_now
        else:
            c_now = np.concatenate((current,b_now),0)
            current = c_now
    return current
s = concatenate_prehdr('SpacecraftTime')

def binner(data, bins):
    while len(data) > bins:
        #if len(data)%2==0:
        data2 = ([ (a+b)/2 for a,b in
        zip(data[::2], data[1::2]) ])
        data = np.asarray(data2)
    #print(data)
    return data

def create_data_prehdr(width):
    sync_data = concatenate_prehdr('Sync')
    #BINNED_bin_data = binner(sync_data,width) ->

```

```

#binner function doesn't work with binary data

length_data = concatenate_prehdr('Length')
BINNED_length_data = binner(length_data,width)

PacketID_data = concatenate_prehdr('PacketID')
BINNED_PacketID_data = binner(PacketID_data,width)

GlobalCount_data = concatenate_prehdr('GlobalCount')
BINNED_GlobalCount_data = binner(GlobalCount_data,width)

Time_secs_data = concatenate_prehdr('Time(secs)')
BINNED_Time_secs_data = binner(Time_secs_data,width)

Time_subsecs_data = concatenate_prehdr('Time(subsecs)')
BINNED_Time_subsecs_data = binner(Time_subsecs_data,width)

LocalCount_data = concatenate_prehdr('LocalCount')
BINNED_LocalCount_data = binner(LocalCount_data,width)

LocalTotal_data = concatenate_prehdr('LocalTotal')
BINNED_LocalTotal_data = binner(LocalTotal_data,width)

SpacecraftTime_data = concatenate_prehdr('SpacecraftTime')
BINNED_SpacecraftTime_data = binner(SpacecraftTime_data,width)

dtp = np.dtype([
    #('Sync'           , 'S30'  ),
    ('Length'         , '<u4'  ),
    ('PacketID'       , '<u4'  ),

```

```

    ('GlobalCount'           , '<u4'  ),
    ('Time(secs)'           , '<u4' ),
    ('Time(subsecs)'       , '<u4'  ),
    ('LocalCount'          , '<u4'  ),
    ('LocalTotal'          , '<u4' ),
    ('SpacecraftTime'     , '<u4' )
    ])

```

```

bpdata= np.rec.fromarrays([
    #sync_data, #SHOULD BE BINNED DATA but
    # there's a bug currently (binner function not
    #compatible with binary files)
    BINNED_length_data,
    BINNED_PacketID_data,
    BINNED_GlobalCount_data,
    BINNED_Time_secs_data,
    BINNED_Time_subsecs_data,
    BINNED_LocalCount_data,
    BINNED_LocalTotal_data,
    BINNED_SpacecraftTime_data], dtype= dtp)

return bpdata

```

```

create_data_prehdr(1)

```

```

def create_data_hdr(width):

```

```

    ''' hard coding this since for now '''

```

```

    bin_data = concatenate_hdr('bin')

```

```

    BINNED_bin_data = binner(bin_data, width)

```

```

sxm_period_data = concatenate_hdr('sxm_period')
BINNED_sxm_period_data = binner(sxm_period_data, width)

TotalEventsCnt_data = concatenate_hdr('TotalEventsCnt')
BINNED_TotalEventsCnt_data = binner(TotalEventsCnt_data,
width)

underflowEventCnt_data = concatenate_hdr('underflowEventCnt')
BINNED_underflowEventCnt_data = binner(underflowEventCnt_data,
width)

overflowEventCnt_data = concatenate_hdr('overflowEventCnt')
BINNED_overflowEventCnt_data = binner(overflowEventCnt_data,
width)

scTime_subsecs_data = concatenate_hdr('scTime(subsecs)')
BINNED_scTime_subsecs_data = binner(scTime_subsecs_data,
width)

scTime_secs_data = concatenate_hdr('scTime(secs)')
BINNED_scTime_secs_data = binner(scTime_secs_data,
width)

scGlobalCount_data = concatenate_hdr('scGlobalCount')
BINNED_scGlobalCount_data = binner(scGlobalCount_data,
width)

dt = np.dtype([
    ('sxm_period',          , '<u2' ),
    ('TotalEventsCnt',    , '<u2' ),

```



```

('underflowEventCnt'          , '<u2'  ),
('overflowEventCnt'          , '<u2'  ),
('bin'                        , '<u2',(512,)),
('scTime(subsecs)'           , '<f8'  ),
('scTime(secs)'              , '<f8'  ),
('scGlobalCount'             , '<f8' )
])

```

```

bdata= np.rec.fromarrays([
    BINNED_sxm_period_data,
    BINNED_TotalEventsCnt_data,
    BINNED_underflowEventCnt_data,
    BINNED_overflowEventCnt_data,
    BINNED_bin_data,
    BINNED_scTime_subsecs_data,
    BINNED_scTime_secs_data,
    BINNED_scGlobalCount_data], dtype= dt)

```

```

return bdata

```

```

def create_file(width, filename):
    bdata = create_data_hdr(width)
    bpdata = create_data_prehdr(width)
    with h.File(filename, 'w') as f:
        grp = f.create_group("data")
        subgrp = grp.create_group("tlm_sxm_data")
        sub2 = subgrp.create_dataset("hdr", data=bdata)
        sub3=subgrp.create_dataset("pre_hdr", data=bpdata)
        f.close()

    return

```

```
create_file(500, 'rebinned_data.h5')
```

### B.3 LTSpice Simulation Readout

This code is used to analyze LTSpice simulation data. LTSpice software was updated between the time early LTSpice readout code written by Dr. Branden Allen, and the SXM low count rate root cause investigation. The code was updated to take .txt files instead of .raw files, which was the old LTSpice file output.

```
#!/usr/bin/env python
#-*- encoding=utf-8-*-
'''
A library for loading the output spice simulations

Author: Branden Allen
Date: 2015.06.18
Edited: Andrew Cummings
Date: 2019.01.30
'''

from __future__ import print_function

#Numerical
import numpy as np

#Standard
import struct
import re

#####
```

```

def open_spice(filename , dtype= 'f'):
    with open(filename , 'rb') as f:
        d= f.read()
        div= re.search('Binary:'.encode(), d)
        data= d[div.end()+1:]
        hdr= d[:div.end()+1]

        #Extract the data
        size= [re.search(i.encode(), hdr).span() for i in
        ['No. Points:\s+\d+', 'No. Variables:\s+\d+']]
        nrow, ncol= [int(hdr[i[0]:i[1]].split(':')[0].encode())-1]
        for i in size]
        #print(nrow, ncol)
        d= np.reshape(struct.unpack(nrow*ncol*dtype, bytearray(5952)),
        (nrow, ncol)) #[1:]

        #Retrieve the data keys
        start= re.search('\nVariables:', hdr.decode()).end()+1
        end= re.search('\nBinary:', hdr.decode()).start()
        keys= [i.split() for i in hdr[start:end].decode().split('\n')]

        #Generate record array
        d= np.rec.fromrecords(d, names= [i[1] for i in keys])
        return d

# Andrew's Version for txt files
def open_text(filename):
    with open(filename , "r") as readfile:
        x=[]

```

```
y=[]

for line in readfile:
    Type = line.split("\t")
    x.append(Type[0])
    y.append(Type[1])
xlabel = x[0]
ylabel = y[0]
x.pop(0)
y.pop(0)
time = np.array(x, dtype=np.float32)
time = time*1.e6
value = np.array(y, dtype=np.float32)
print(xlabel , ylabel)
return time , value
```

#####